

For Reference

NOT TO BE TAKEN FROM THIS ROOM

For Reference


NOT TO BE TAKEN FROM THIS ROOM

Ex libris
UNIVERSITATIS
ALBERTAENSIS



Regulations Regarding Theses and Dissertations

[illegible]



Digitized by the Internet Archive
in 2023 with funding from
University of Alberta Library

<https://archive.org/details/Hemmings1969>

Thesis
1969(F)
101

THE UNIVERSITY OF ALBERTA

UPPER MANTLE STRUCTURE IN WESTERN CANADA

by



CHARLES DAVID HEMMINGS

A THESIS

SUBMITTED TO THE FACULTY OF GRADUATE STUDIES
IN PARTIAL FULFILMENT OF THE REQUIREMENTS FOR THE DEGREE
OF MASTER OF SCIENCE

DEPARTMENT OF PHYSICS

EDMONTON, Alberta

FALL, 1969

UNIVERSITY OF ALBERTA
FACULTY OF GRADUATE STUDIES

The undersigned certify that they have read,
and recommend to the Faculty of Graduate Studies for
acceptance, a thesis entitled UPPER MANTLE STRUCTURE
IN WESTERN CANADA submitted by Charles David Hemmings
in partial fulfilment of the requirements for the degree
of Master of Science.

ABSTRACT

Refraction arrivals from the upper mantle were recorded on a 3500 km. profile stretching from Lake Superior to Alaska. Recordings from the middle section of the profile (1000 - 2000 km.) were digitized, and various frequency and velocity filters were used to enhance this data. One version of the velocity filter, a non-linear operator, obtained the highest degree of data enhancement, but at the expense of signal distortion. The analysis presented in this paper rests primarily on these enhanced records and secondarily on the analog records.

The velocity structure was obtained by matching a theoretical travel time curve calculated from proposed structures to the observed travel time curve. The most successful model thus produced was model U of A #3. This model contained four striking features; two velocity reversals, one at a depth of 42 to 70 km. and the other at 125 to 170km., both of which were followed by rapid velocity increases, and two rapid velocity increases at depths of 455 and 660 km. These velocity reversals were necessary to reproduce the shadow zone at a distance of 900 km. and its accompanying cusp at 300 km., and the shadow zone at 1500 km. with its cusp at 800 km. The rapid velocity increases were used to produce two cusp

pairs, the first at 3200 and 1700 km., and the second at 3300 and 2200 km. Two additional velocity reversals at depths of 198 to 230 km. and 250 to 325 km. with a small velocity increase between them were needed to produce the shadow zones at 2000 and 2400 km. respectively. These reversals were too small to produce any detectable cusping.

To complete the details of this structure, and to obtain the velocity behaviour in the transition zones, the theoretical amplitudes calculated from the model must be made to match the observed amplitudes. This amplitude study is not presented in this paper. However, the computer program listed in the appendix calculates both amplitudes and travel times, and is presently being used to complete this study.

ACKNOWLEDGEMENTS

I take great pleasure to have this opportunity to thank Dr. E. R. Kanasewich for the constant encouragement and guidance provided by him throughout my entire course of study at the University of Alberta.

I would also like to thank Dr. G. L. Cumming for his work during the initial stages of Project Early Rise.

A special vote of thanks to the technicians and field personnel, from both the University of Alberta and the United States Geological Survey, for their diligence in recording and digitizing the data, which is the backbone of any seismic research.

Financial support for this research was supplied by the United States Air Force (Grant # AF-AFOSR-1140-66) through the offices of the Arctic Institute of North America.

Throughout this study, the author was supported by Graduate Teaching and Research Assistantships from the Department of Physics, University of Alberta, and a bursary from the National Research Council of Canada (Grant # A2633).

I would like to thank the University of Lethbridge for their help in printing this paper, particularly Mr. Boon.

Finally, I would like to dedicate this thesis to my wife, Betti. Without her constant understanding and support this thesis would not have been completed. Also, I wish to acknowledge the work she has done on this paper, which involved, among other things, the proof-reading and typing of the manuscript.

TABLE OF CONTENTS

Abstract	iii
Acknowledgements	v
List of Illustrations	ix
Chapter 1. Data Collection	1
1.1 Introduction	1
1.2 Planning	1
1.3 Field Equipment	7
1.4 Field Operation	8
1.5 Digitization	11
1.6 Bookkeeping and Data Limitations	13
Chapter 2. Data Enhancement	15
2.1 Introduction	15
2.2 Detection and Elimination of Spurious Transients	16
2.3 Frequency Filtering	17
2.4 Linear and Non-Linear Beamforming	18
2.5 Display of Results	32
Chapter 3. Data Interpretation	38
3.1 Earth Model - Ray Theory	38
3.2 Solutions of the Ray Path Integrals	46
3.3 Ray Flux Calculations	56
3.4 Interpretation of the Travel Time Curve	67

Bibliography	67
--------------	----

Appendix. Fortran IV Program for the Time and Distance Integrals	A.1
---	-----

LIST OF ILLUSTRATIONS

Figure 1.1	Project Early Rise.	3
1.2	The Western Canada profile.	5
1.3	Frequency response of the Hall-Sears HS-10 seismometers.	9
1.4	Frequency response of the Texas Instruments vertical S-36 seismometers.	10
2.1	Impulse response in the time domain for a four pole zero phase Butterworth 1.0 - 5.0 HZ band pass filter.	19
2.2	Impulse response in the frequency domain for a four pole zero phase Butterworth 1.0 - 5.0 HZ band pass filter.	20
2.3	Impulse response in the time domain for a four pole zero phase Butterworth 0.5 - 3.0 HZ band pass filter.	21
2.4	Impulse response in the frequency domain for a four pole zero phase Butterworth 0.5 - 3.0 HZ band pass filter.	22

Figure 2.5	Five records covering the range 1128 to 1472 km. before data enhancement.	23
2.6	These same records after applying the 1.0 - 5.0 HZ Butterworth band pass filter.	24
2.7	These same records after applying the 0.5 - 3.0 HZ Butterworth band pass filter.	25
2.8	These same records after applying the velocity filter.	26
2.9	These same records after applying the 8 th root stack filter.	27
2.10	Spike attenuation using the N th root stack on K channels of input.	33
2.11	Composite plot of velocity filtered records.	36
2.12	Composite plot of 8 th root stack filtered records.	37
3.1	Diagram of a ray passing through an earth made up of homogeneous concentric shells.	39

Figure 3.2	Center point integration formula approximation to the area under the curve.	55
3.3	Diagram of two rays passing through the earth, showing the change in the angular displacement of the emerging ray for a small change in the angle of incidence.	58
3.4	Ray diagrams for body waves passing through earth models U of A #1 and U of A #3.	61
3.5	Velocity and travel time curves of the Lewis and Meyer model and the University of Alberta model U of A #1. Also shown are the observations of the first events and a prominent secondary event of the Western Canada profile.	62
3.6	Velocity and travel time curves of the models U of A #2, U of A #3, and U of A #3a along with the Western Canada profile observations.	63

- Figure 3.7 Ray diagram for body waves passing
through the earth model U of A #2. 65
- 3.8 Velocity and travel time curves of the
final model produced by the University
of Alberta (U of A #3) along with those
resulting from the oceanic model
produced by Johnson and the average
crustal model produced by Herrin,
Tucker, Taggart, Gordon, and Lobdell. 66

CHAPTER 1.

DATA COLLECTION

1.1 Introduction

Project Early Rise, sponsored by the United States Air Force Office of Scientific Research and coordinated by the United States Geological Survey, was an experiment designed for the investigation of the upper mantle using seismic body waves. In previous studies, earthquakes and nuclear explosions were used as the seismic source. However, due to the nature of these sources, the resulting refraction profiles were often in anomalous areas and were necessarily short or sparsely occupied. Also, the source parameters, such as origin time, hypocenter, energy, and transfer function, were not always well known, which added further confusion to the complex travel time and amplitude curves for seismic body waves. For a successful experiment, the profiles had to be long and detailed, with as many of the source parameters independently measurable or known as possible. Project Early Rise was planned to meet these requirements.

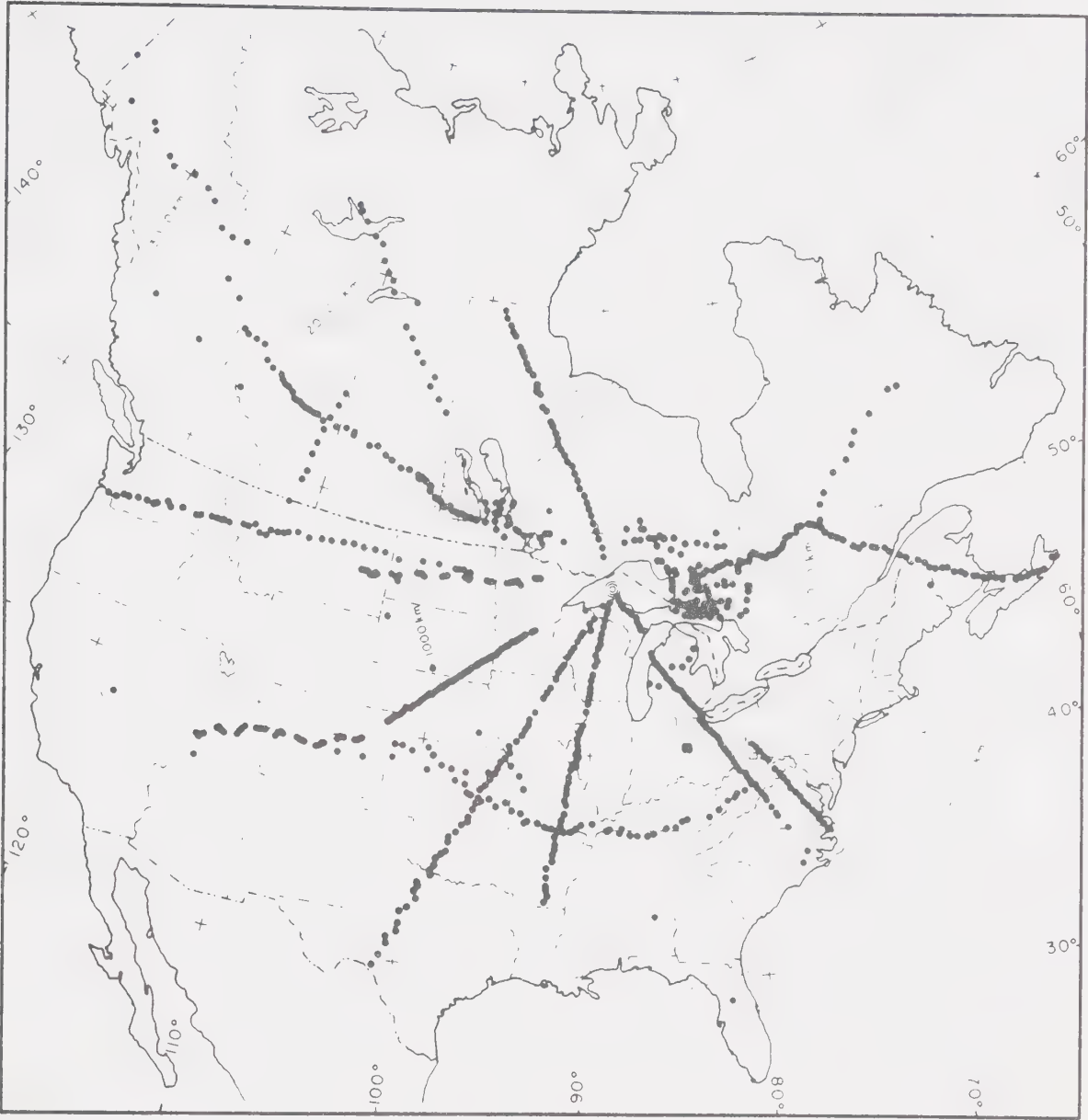
1.2 Planning

Probably never before had such a wealth of

information been available for the planning of a refraction program. Cumming and Kanasewich (1965) demonstrated the feasibility of using underwater chemical explosions of a reasonable size as the seismic source for upper mantle investigation. They recorded several of the two to ten ton shots from the 1963 Lake Superior crustal experiment at distances sufficiently great (1600 - 1900 km.) that the seismic waves producing the first events had penetrated the mantle. This experiment also provided a known crust (Berry and West, 1966) under Lake Superior and provided data regarding seismic coupling of underwater explosions at various locations within the lake. Underwater shots had a second advantage due to the fact that all shots could be set off at the same location, thus yielding a common transfer function, coupling, and crust for all explosions. The same experiment provided valuable experience in shot procedure. Most important, it resulted in a proven system of hydrophone stations for measuring the shot instant and precise shot location. The 1963 experiment, as well as another one in 1964, guaranteed a reliable source with accurately measurable source parameters.

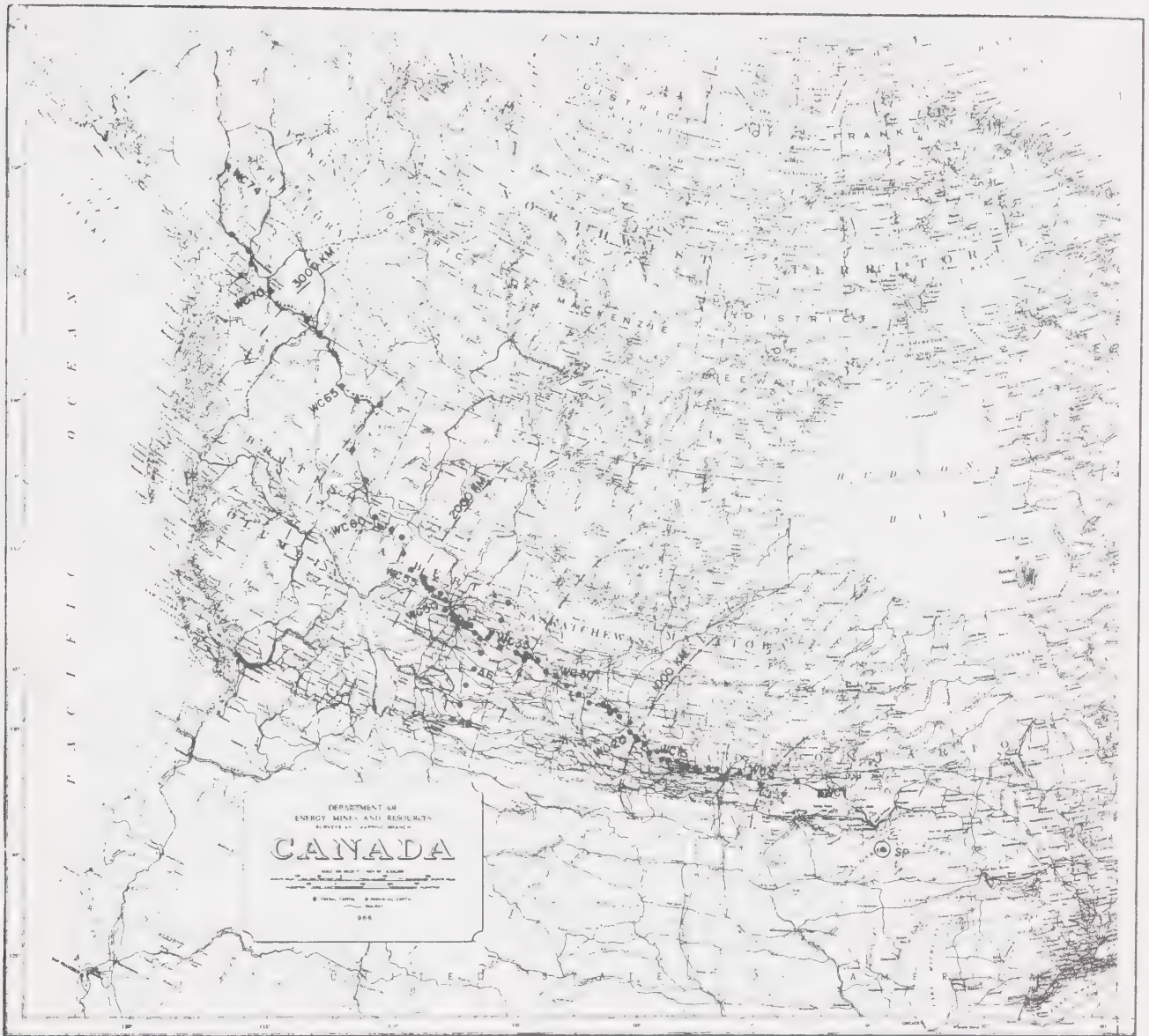
As a result of these studies, forty shots of five tons each were detonated at a common shot point in July 1966 during Project Early Rise. These formed the sources for the many seismic profiles, shown in figure 1.1, undertaken by various university and government research

Figure 1.1 Project Early Rise.



laboratories. Five seismic crews, two from the University of Alberta and three from the United States Geological Survey (USGS), employing mobile linear arrays, participated in the Western Canada (WC) profile, consisting of 74 recording sites running along a WNW line (figure 1.2). The first site was 400 km. from the shot point and the last 3600 km. In addition, 9 sites made up an arc 1675 km. from the shot point. Stretching from Cold Lake, Alberta, to just south of the Trans Canada Highway near Suffield, Alberta, this arc encompassed approximately 20 degrees. Generally, the spacings between sites was 50 km., which was increased beyond the range of 2000 km. It was felt that this spacing would preserve the signal character from one site to the next, and this character could then be used to trace events across the profile. Near Holden, Alberta, from 1754 km. to 1781 km., the spacing was reduced to the length of the array (2 miles). This continuous section of the profile was to provide data over an anticipated critical distance for arrivals from below a possible low velocity layer in the mantle, and was to be used for experiments in beam forming. In addition, two permanent sites were occupied for the duration of the experiment, one at the University of Alberta Edmonton Seismic Observatory near Leduc, Alberta (1840 km.), and the other at the intersection of the profile and the arc (WC 36). These stations were expected to supply data for stacking and for calibrating the spectral density estimates

Figure 1.2 The Western Canada profile.



of the individual sources.

The proposed recording sites were taken from large scale maps (4 miles = 1 inch) and located on isolated EW roads. It was the responsibility of the recording crews to make the final selection of the recording locations when they arrived on the proposed site on the day it was to be occupied. In choosing the final site locations, the crews had to consider such features as power lines and seismic background noise, while maintaining the proposed spacings on the profile. Since these were small, it was considered best if each crew worked a particular range of the profile. In this way they could consider the final location of the previously occupied site in choosing the new one, thus preserving the planned spacings. The crews also had to estimate the recording times at each location. Initially they used a velocity of 8.2 km./sec. and an intercept time of +5 seconds to estimate the arrival times, as taken from a review of the Cumming and Kanasewich data. These times were to be modified and the recording gains adjusted by extrapolating the data collected during the exercise. On the other hand, crews occupying adjacent sites would have more information on which to base these decisions, and an experienced observer could review all the records and make these decisions while the crews slept. Also, one technician could then service all of the recording equipment. Ideally, of course, these two

specialists would have no recording responsibilities.

Both systems were employed. The three USGS crews occupied adjacent sites on the close range section of the profile (400 to 1000 km.), after which each crew took on profile assignments on the far section (2000 to 3600 km.) The University of Alberta crews were given profile assignments on the central section of the profile (1000 to 2000 km. including the arc). Both systems worked well. It was found that the freedom of site selection offered by the profile section assignments was extremely valuable in the selection of good sites. However, due to the quality of data and the lack of time for adequate analysis, weak first arrivals were not always observed by the field parties, and hence no allowance was made for recording them on subsequent days. This type of oversight proved a handicap in the final data analysis, and could possibly have been avoided had the adjacent site method been used.

1.3 Field Equipment

The USGS crews employed their standard mobile 6 station linear array refraction equipment. The University of Alberta crews used their mobile 12 station refraction / reflection linear array apparatus, the same as used by Maureau (1964) during his crustal refraction program and by Clowes (1966, 1969) during his deep crustal reflection programs. The latter arrays consisted of 12

stations with spacings of 960 feet covering 2 miles. At station 6, as numbered from one end of the array, the leads of stations 2 and 4 were tapped, and a three component (vertical, radial, and transverse) station was established using Hall-Sears HS-10 seismometers. Elsewhere, other than at 2 and 4, Texas Instruments vertical S-36 seismometers were employed. See figures 1.3 and 1.4 for the seismometer responses. All components of the array, in addition to timing information, were recorded on a RS-8U recording oscillograph. These records will hereafter be referred to as the field monitor records. A Precision Instrument PS 207 AM/FM seven channel tape deck was used to record 6 components of the array in FM, and one channel of timing information in AM. Two modes of recording were available, one recording the odd numbered array components, hereafter referred to as the normal mode, and another, the reverse mode, recording the even components. Thus either a 6 station or a 4 station (having in addition the two horizontal components) linear array, both with spacings of 1920 feet, were available for replay and digitization in the Edmonton laboratory.

1.4 Field Operation

The field operation, then, entailed the location of a noise-free site, setting up the array and the recording equipment, and recording the shot. Noise records were

Figure 1.3 Frequency response of the Hall-Sears HS-10
seismometers.

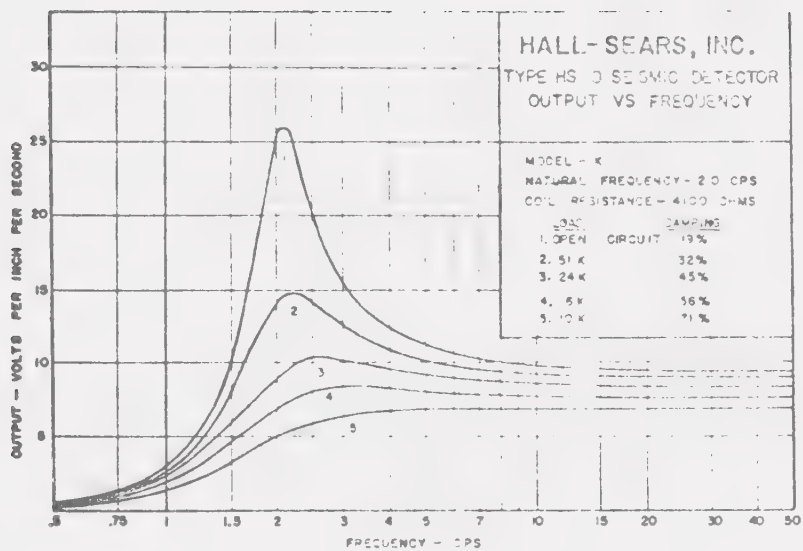


Figure 1.4 Frequency response of the Texas Instruments
vertical S-36 seismometers.

TI S-36

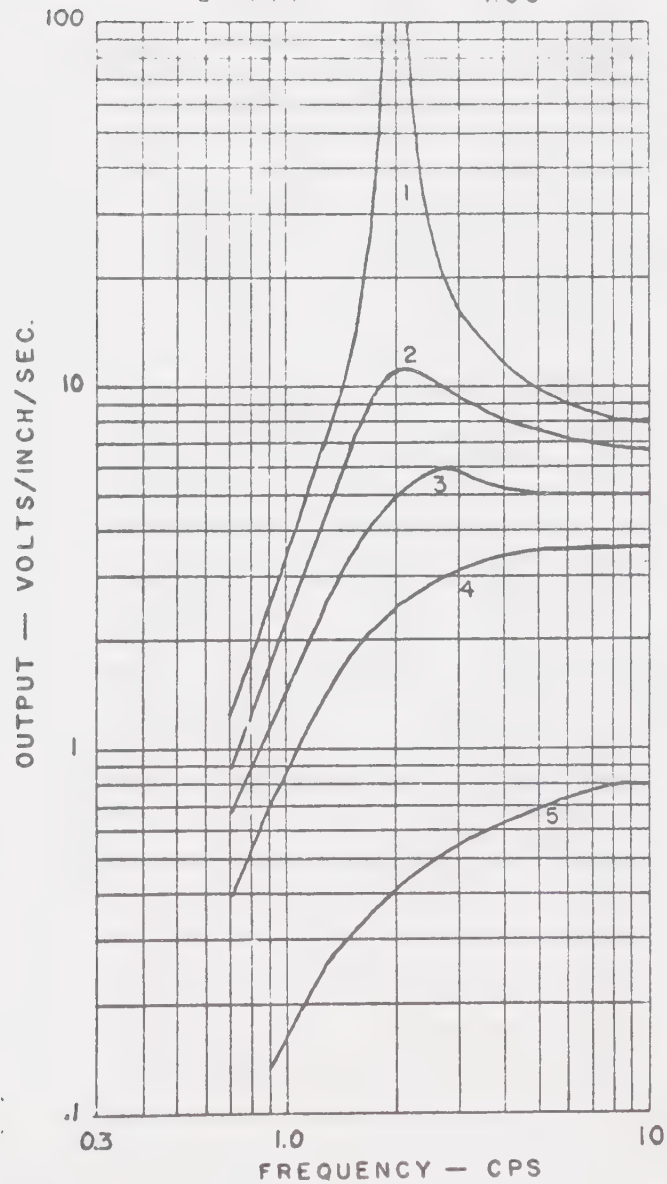
NATURAL FREQUENCY — 2 CPS

COIL RESISTANCE — 4K OHMS

LOAD

DAMPING

1. INFINITE	0
2. 15 K	.311
3. 6 K	.500
4. 2.6 K	.707
5. 444	1.00



run to determine the state of the system and the background noise level at different filter frequencies. These recordings were run several times. Once before the system was completely set up, leaving ample time for repairs or site relocation, and again as soon as the station was in the ready state, in order to determine attenuations and filter settings for the recording of the shot. The first shot was recorded in the normal mode, using the data collected at previously occupied sites as a guide for recording times and attenuations. The record quality and the arrival times of this record were then checked on the field monitor record and used as a guide to record the second shot of the day, which was recorded at the same site. The second shot could be recorded in the reverse mode by reversing the array cable inputs; hence the name, reverse mode. Top priority was placed on the normal mode recording, as it provided the largest array on tape. If the first shot record was of good quality, the second shot of the day, at alternate sites only, was recorded in the reverse mode. A day's operation consisted of the recording of two shots on both tape and photographic paper.

1.5 Digitization

The digitizing system consisted of a 6 channel hot wire recorder for monitoring the tape channels, a

two channel pen recorder for the tape timing channel and the digitizing time, aliasing filters, a 6 channel Packard Bell multiplexer, a Packard Bell 11 bit analog to digital converter, a clock (a square wave oscillator which governed the conversion rate), a digital counter, switching circuit between two Kennedy digital tape recorders, and the PS 207 tape deck in the replay mode. Because the system was not designed to convert and record seismic data rapidly enough (over 100 samples per second (s/s) per channel were required for statistical significance, requiring 600 s/s by the system), the FM tape which was recorded at 30 inches per second (i/s) was replayed at $3\frac{3}{4}$ i/s.

Thus the digitizing time was increased a factor of 8 over real time, and a conversion rate of 90 s/s digitizing time was equivalent to 120 s/s per channel real time, which slightly exceeded the required rate. The aliasing filter, 24 db per octave, corner frequency of 4.0 HZ digitizing time was used to assure that there was no signal of any significant power at a frequency higher than the aliasing frequency (7.5 HZ machine time). It should be noted that the data was recorded using a 24 db per octave filter with a corner frequency of 8 to 16 HZ which corresponds to 1 HZ to 2 HZ in digitizing time. Thus any signal near or above the aliasing frequency was severely attenuated.

The data was digitized in channel sequence with

a flag marker added to the word of the sixth channel, and was recorded on the digital tape in this form. This was organized into records consisting of 10 blocks of 3600 words each, giving a total of 36000 words per record or 6000 words per channel (just over 50 seconds real time of seismic data). Inter-record gaps are required between blocks. As the Kennedy recorders demanded more time to insert these than the sampling interval, two recorders and a switching circuit were used. When one recorder had recorded a full block, it put in its inter-record gap while the other recorder recorded the next block. This solution was considerably less expensive than using a high speed memory bank interfacing system. Thus each FM tape was digitized and recorded on two digital tapes.

The data was taken in this form to the IBM 360 Model 67 computer, and one tape containing all the data was built. During this process, longitudinal and horizontal parity checks and channel sequence checks, along with other IBM system checks, were made to insure that the digital data was reliable. On detection of an error the data was rejected and later redigitized. In this manner 114 digital records were compiled on two master tapes.

1.6 Bookkeeping and Data Limitations

Before data analysis could begin, a considerable amount of bookkeeping had to be done. The locations of the

shot points were taken from a technical letter published by the United States Geological Survey (Warren, Healy, Hoffman, Kempe, Rauula, and Stuart; 1967), and the recording sites were determined from large scale maps. From this, the profile distances were calculated using a Fortran program based on a Clarke spheroid model of the earth. The accuracy of the distances was limited to the scale of the map and was estimated to be 0.2 km. Time was synchronized between the shot point and the recording crews to an accuracy of 0.005 second using WWV as a standard. Irregularities in the spreads were noted in the field log books, and the spread configurations calculated to the nearest 2 meters. The digital data was plotted on the CalComp model 663 plotter using the same time and amplitude scales as those of the field monitor records. From a direct comparison of the two, the time of beginning and end of digitization was measured and the sampling interval calculated. Using this data, the timing of events could begin.

CHAPTER 2.

DATA ENHANCEMENT

2.1 Introduction

Any signal consists of two parts, one being wanted and the other unwanted, the latter being defined as noise. The noise can be broken down into various categories, depending on its characteristics; in fact, the noise signal can be considered as a combination of several types. The superposition theorem tells us that we can treat the wanted signal and each type of noise as separate signals. Signal enhancement, then, consists of the separation of these components, or at least the suppression of the noise.

Various processes have been derived for signal detection and noise rejection. These methods fall under two main headings, one being analog and the other digital. In general, for every analog process there exists an equivalent digital one, and vice versa. Thus this is not a true classification of procedures, but a classification of signal format and of the machine used to execute the procedure.

It becomes a question of which machine to use. Analog computers require separate electronic components

for each operation, such as addition, multiplication, delays, etcetera, and wires for controlling the operation sequence. The machines tend to be expensive and very specialized, with more noise being added to the signal by each amplifier. In digital computers, all operations are broken down into binary operations and the logic is represented by machine instructions generated by a language such as Fortran. Thus one machine can perform all the operations, with the programmer varying the logic as required. Hence the digital computer is extremely versatile and free of noise. The only noise introduced is in the round off of numbers during the binary operations, which may be rendered insignificant. However, because of the flexibility of the computer and the break-down of operations into simpler binary operations, the digital process can be substantially slower than the equivalent analog one. The selection of processes often breaks down into speed versus flexibility. For research purposes, flexibility is far more important, hence the analog signal was digitized and then processed on an IBM 360/67 computer.

2.2 Detection and Elimination of Spurious Transients

Transients or spikes are characterized by their rapid change to a maximum followed by an over-damped return to the normal signal level. These spikes occurred during field recording or during laboratory digitization. A

first difference method was used to detect the rapid change and a linear interpolation to replace the spike. A more sophisticated correction algorithm was not attempted due to the difficulty in establishing a suitable detection criterion. Moderate success was attained using the deviation of the first difference from the mean first difference as established over a two second interval in the record, this window being moved across the entire record. The allowable deviation was based on the standard deviation from the first difference. Once the spike is detected and its amplitude determined, and knowing the time constant and the damping of the system which generated the transient, it should be possible to calculate the transient signal. Thus it can be removed by subtracting the calculated signal from the seismic signal. It appears that it is possible to write an anti-spike algorithm, but the limitation of time prevented its full development.

2.3 Frequency Filtering

Local cultural activity and the wind generated background noise which was generally of a higher frequency than the wanted signal. A Butterworth zero phase band-pass filter, programmed by Alpaslan (1968), was used to reject this noise component. One filter with cut-off frequencies of 1.0 and 5.0 HZ passed nearly all of the signal and attenuated most of the noise. Another filter (0.5 and 3.0

HZ) slightly attenuated the signal and rejected almost all of the noise; however, it also removed the character of the signal. Figures 2.1 to 2.4 show the impulse and amplitude responses of these filters. Figure 2.5 shows some unfiltered Early Rise records, while figures 2.6 and 2.7 show the large improvement after application of these filters.

2.4 Linear and Non-Linear Beamforming

As this background noise was also incoherent, a method of beamforming which is based on this criterion for rejection is the simple delay and add routine. This is a linear method and amounts to timing the antenna (array) to point in a particular direction. The acceptance lobe can be sharpened by using weighting coefficients on each of the signals to be added. This procedure is commonly known as stacking or velocity filtering, as the delays depend on the geophone spacings and the assumed apparent velocity of the wanted arrival. Figure 2.8 shows the results of the before-mentioned records after application of this velocity filter.

Another beamforming technique employed is a non-linear variation of the delay and sum. This method (Muirhead, 1968) consists of a delay, taking the N^{th} root of the signal, summing, and then raising the result to the N^{th} power. Hereafter it will be referred to as the N^{th} root stack. As can be seen in figure 2.9, this technique had

Figure 2.1 Impulse response in the time domain for a
four pole zero phase Butterworth 1.0 - 5.0
HZ band pass filter.

IMPULSE RESPONSE OF BUTTERWORTH BAND PASS FILTER

IN PUT PARAMETERS

M=1 LCF= 1.0
T= 0.0083 HCF= 5.0
Ns 1024.0

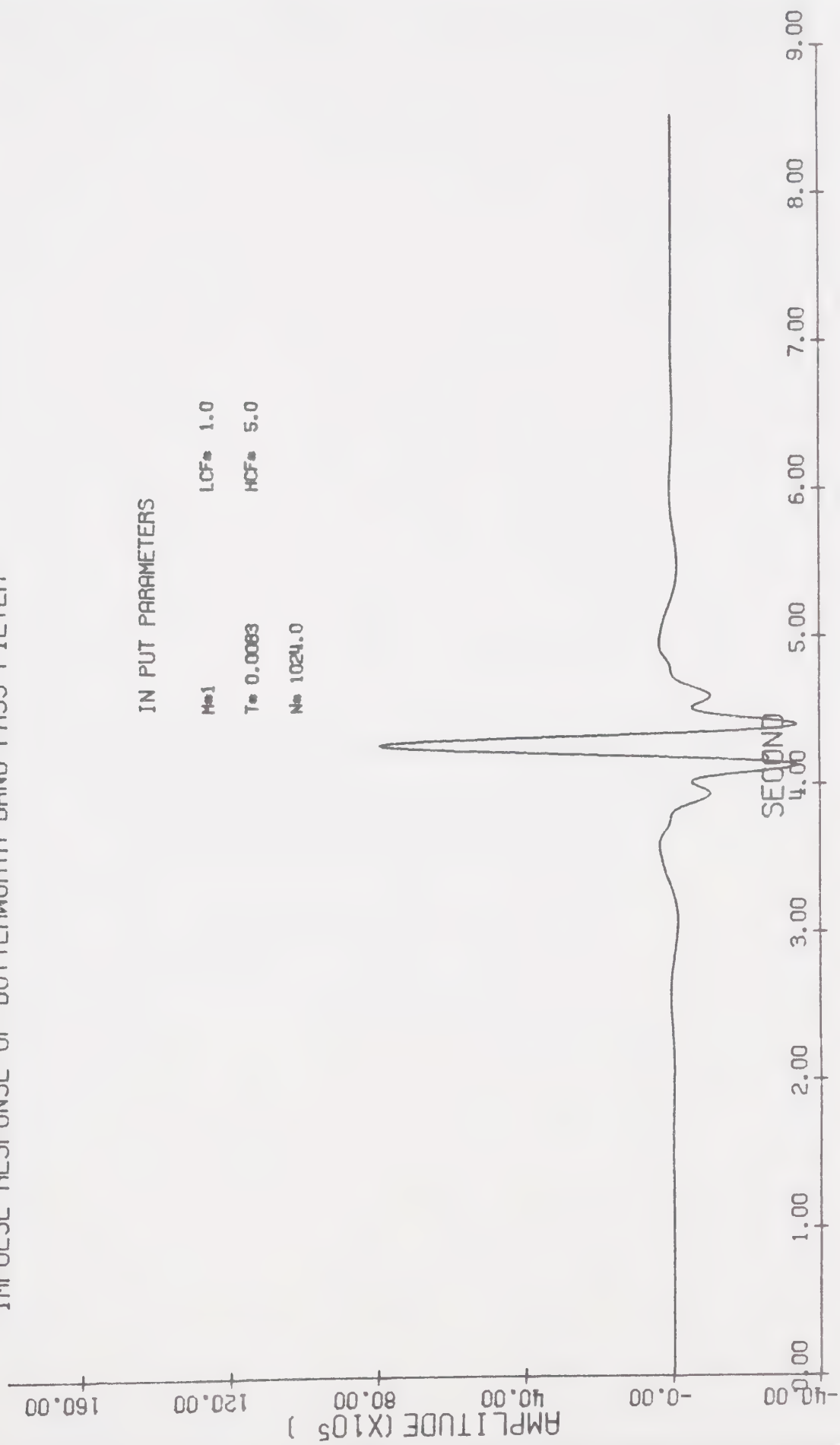


Figure 2.2 Impulse response in the frequency domain
for a four pole zero phase Butterworth
1.0 - 5.0 HZ band pass filter.

AMPLITUDE RESPONSE OF BUTTERWORTH BAND PASS FILTER FOR 1.0 - 5.0 HZ

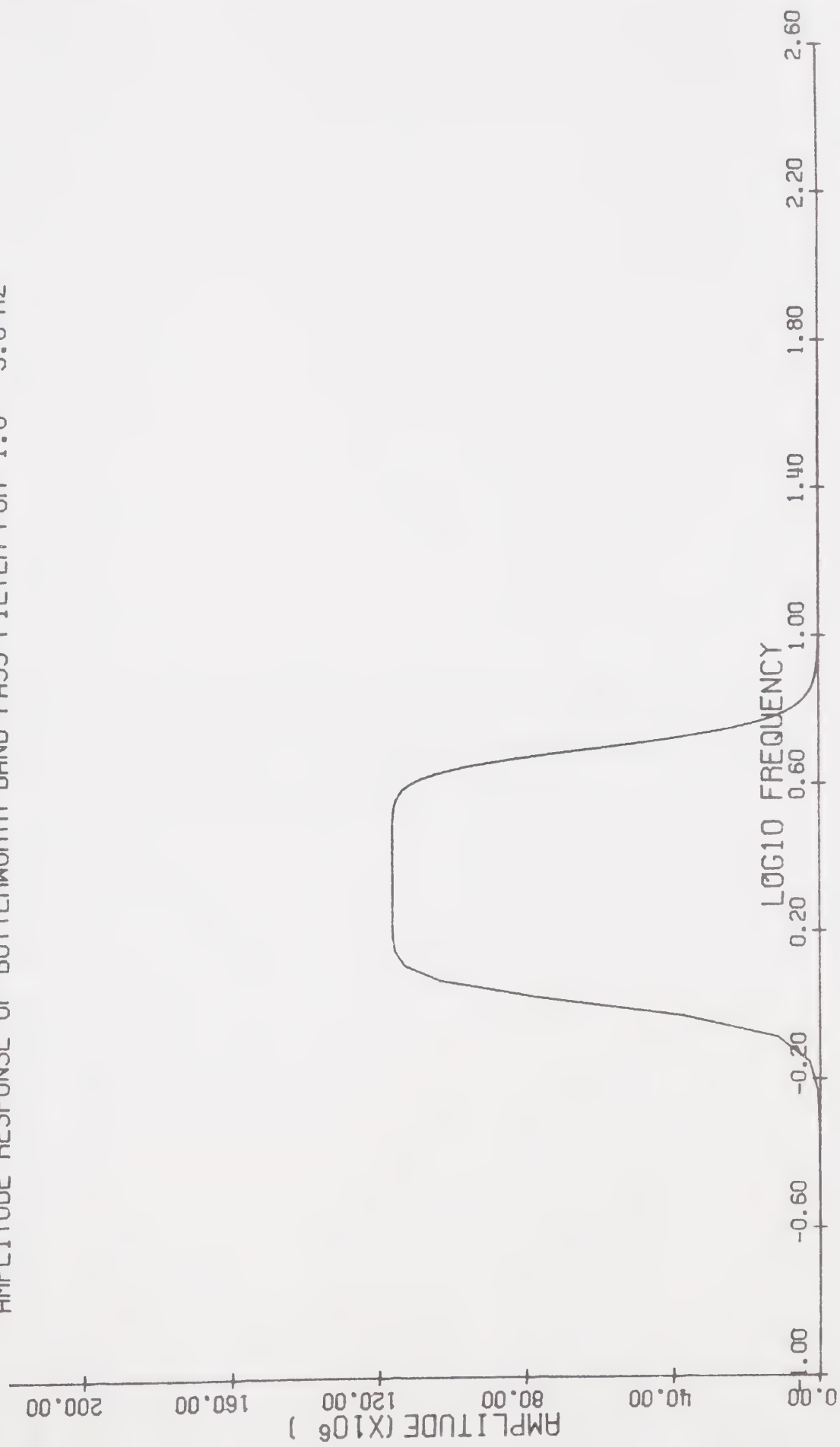


Figure 2.3 Impulse response in the time domain for a
four pole zero phase Butterworth 0.5 - 3.0
HZ band pass filter.

IMPULSE RESPONSE OF BUTTERWORTH BAND PASS FILTER

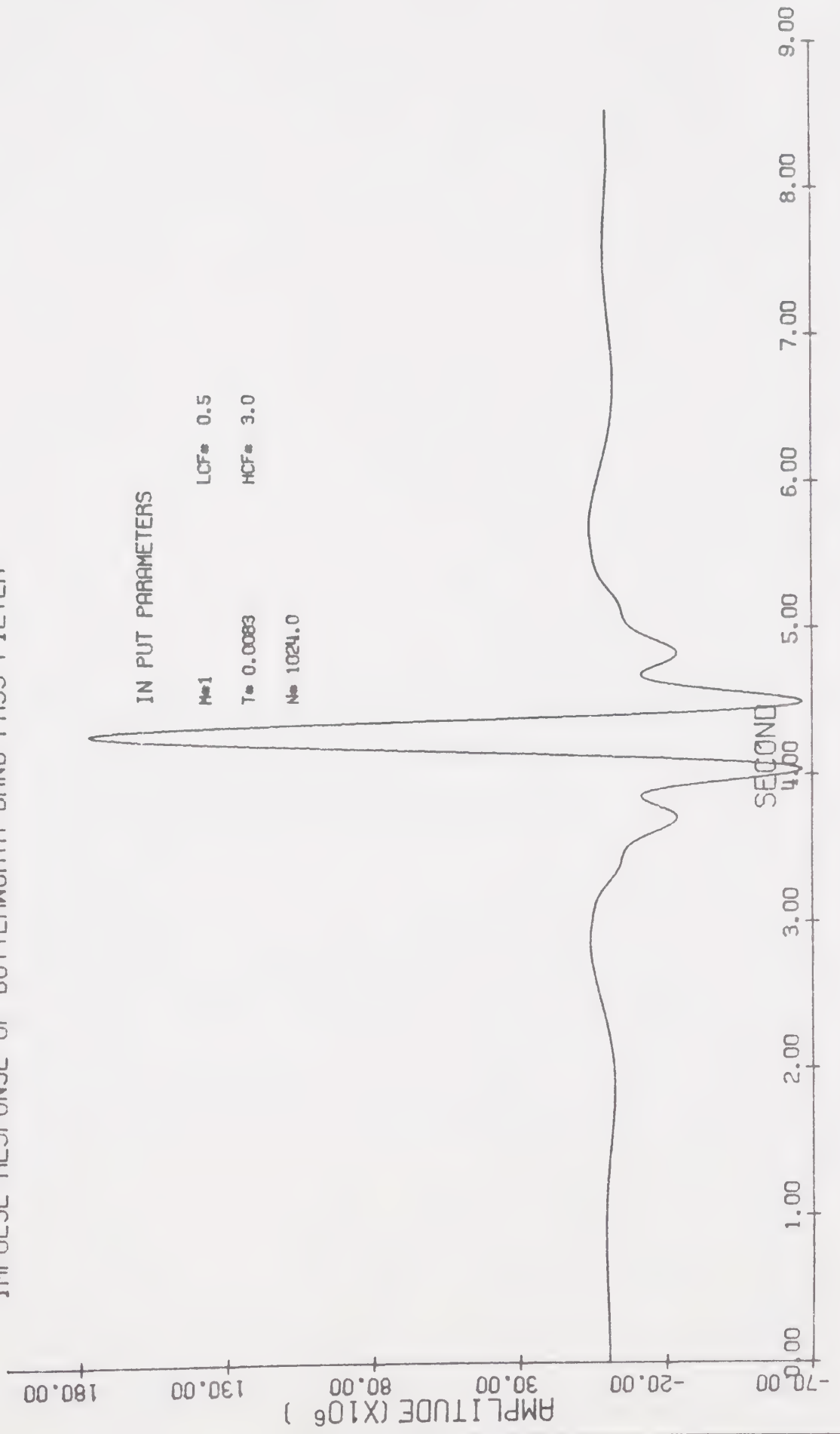


Figure 2.4 Impulse response in the frequency domain
for a four pole zero phase Butterworth
0.5 - 3.0 HZ band pass filter.

AMPLITUDE RESPONSE OF BUTTERWORTH BAND PASS FILTER FOR 0.5 - 3.0 HZ

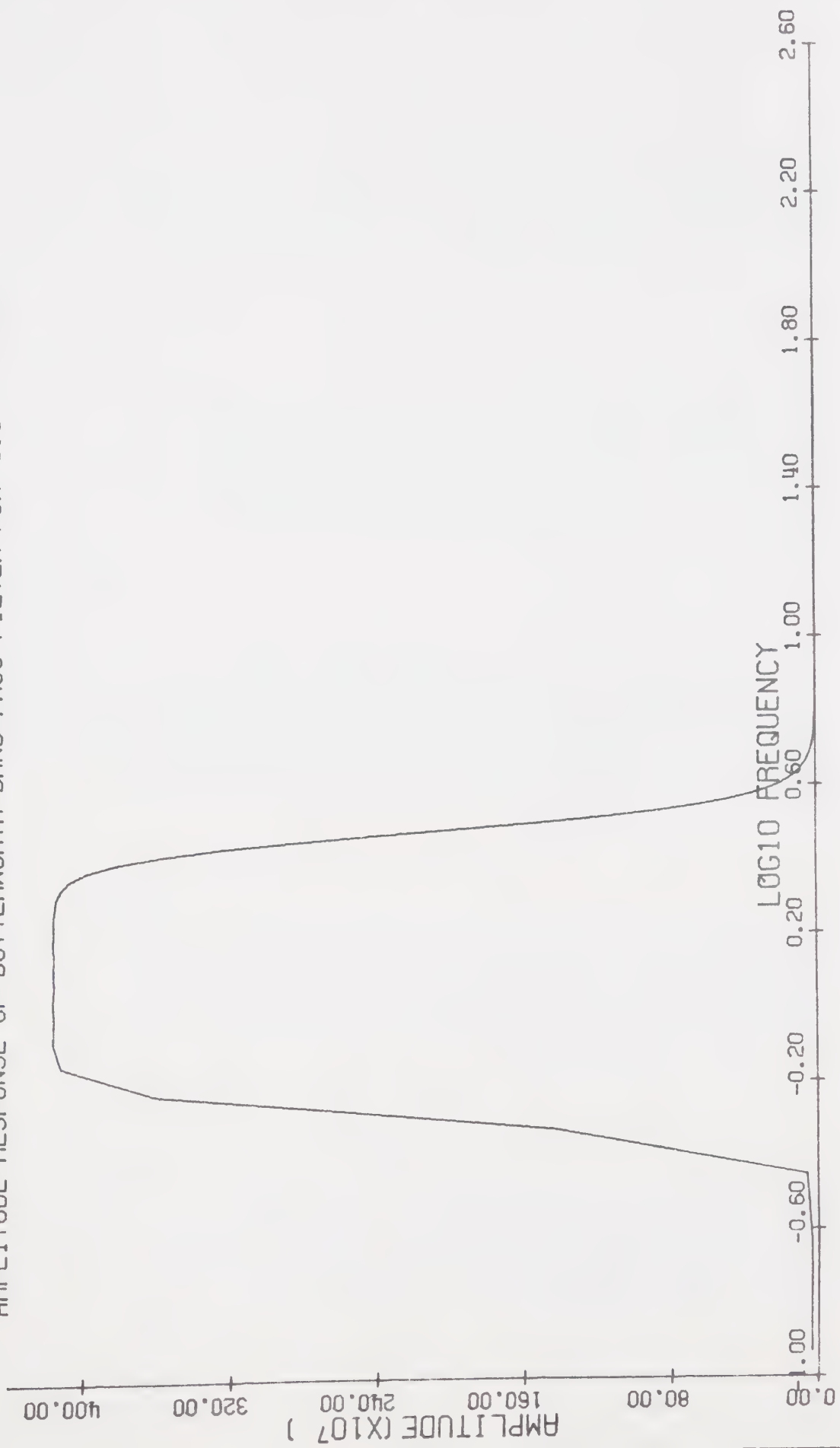


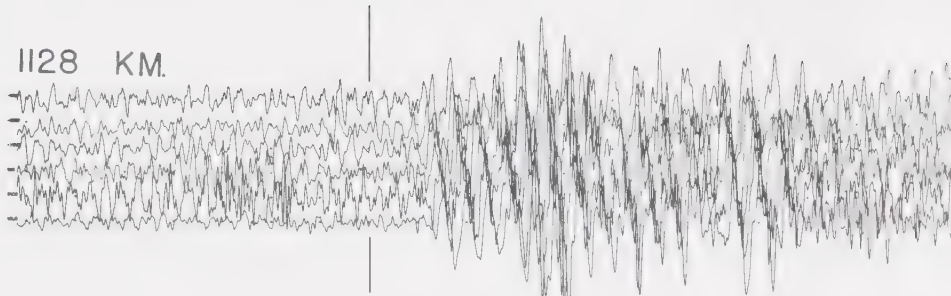
Figure 2.5 Five records covering the range 1128 to
1472 km. before data enhancement.

UNFILTERED

T-DELTA/8.5

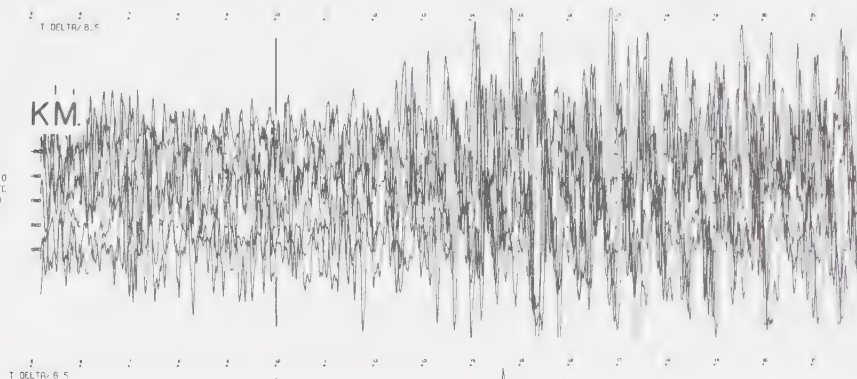
1128 KM.

RECORD 2
MC 25.0 SHOT 4.0
TODIC 2.62 SEC
DELTA 1128.39 KM
ATTN 18.0 DB



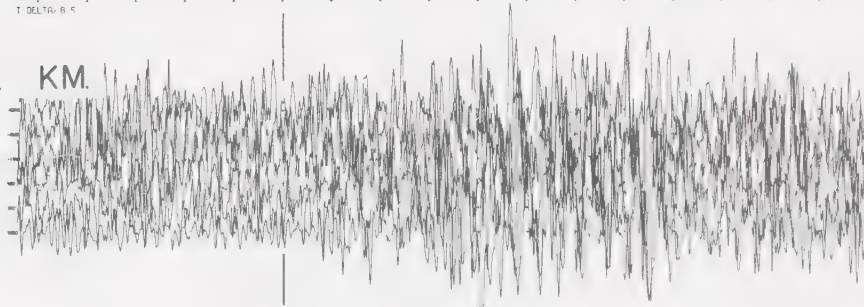
1140 KM.

RECORD 1
MC 24.0 SHOT 3.0
TODIC 5.21 SEC
DELTA 1140.40 KM
ATTN 18.0 DB



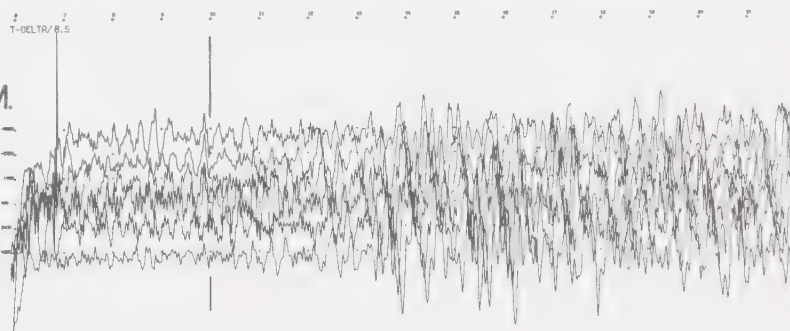
1232 KM.

RECORD 5
MC 27.0 SHOT 6.0
TODIC 4.77 SEC
DELTA 1232.20 KM
ATTN 18.0 DB



1428 KM.

RECORD 3
MC 31.0 SHOT 14.0
TODIC 4.25 SEC
DELTA 1428.47 KM
ATTN 18.0 DB



1472 KM.

RECORD 15
MC 32.0 SHOT 16.0
TODIC 6.95 SEC
DELTA 1472.73 KM
ATTN 18.0 DB

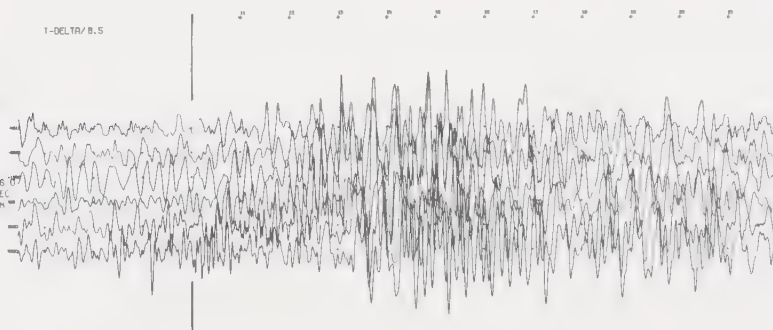


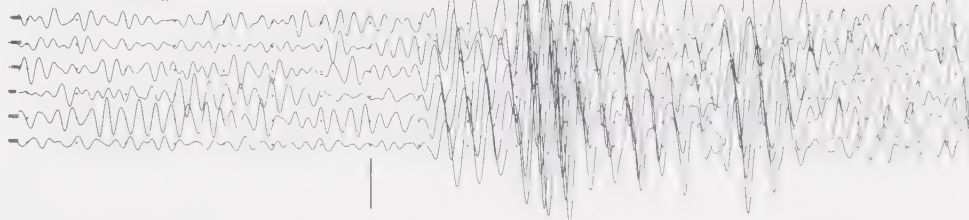
Figure 2.6 These same records after applying the
1.0 - 5.0 HZ Butterworth filter.

BANDPASS 1.0 - 5.0 HZ.

T-DELTA/8.5

1128 KM.

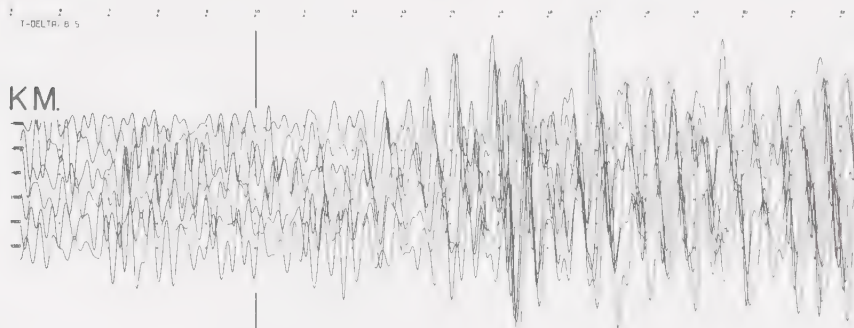
RECORD 2
AC 25.0 SHOT 4.0
T001G 2.82 SEC
DELTA 1128.39 KM
ATTN 18.0 DB
FIL 11.0 5.0



T-DELTA/8.5

1140 KM.

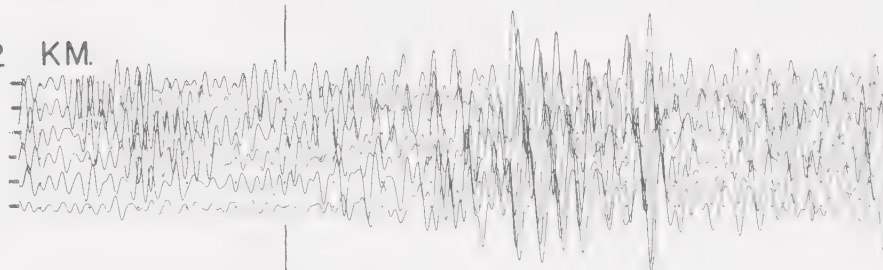
RECORD 1
AC 24.0 SHOT 3.0
T001G 5.21 SEC
DELTA 1140.40 KM
ATTN 18.0 DB
FIL 11.0 5.0



T-DELTA/8.5

1232 KM.

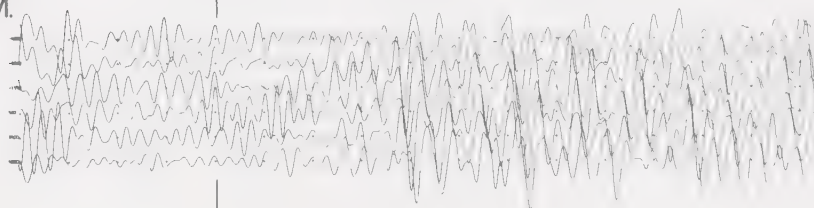
RECORD 5
AC 27.0 SHOT 6.0
T001G 4.57 SEC
DELTA 1232.20 KM
ATTN 18.0 DB
FIL 11.0 5.0



T-DELTA/8.5

1428 KM.

RECORD 3
AC 31.0 SHOT 14.0
T001G 5.45 SEC
DELTA 1428.47 KM
ATTN 18.0 DB
FIL 11.0 5.0



T-DELTA/8.5

1472 KM.

RECORD 15
AC 32.0 SHOT 16.0
T001G 5.45 SEC
DELTA 1472.79 KM
ATTN 18.0 DB
FIL 11.0 5.0

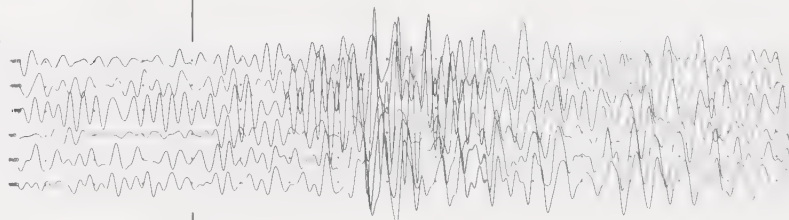


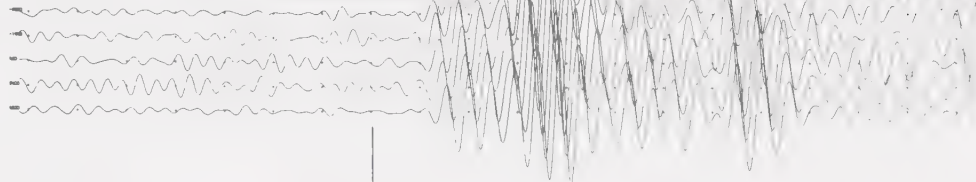
Figure 2.7 These same records after applying the
0.5 - 3.0 HZ Butterworth filter.

BANDPASS
0.5 - 3.0 HZ.

T-DELTA/8.5

1128 KM.

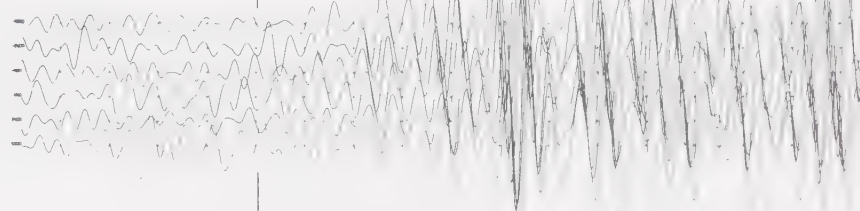
RECORD 2
MC 25.0 SHOT 9.0
TODIC 2.57 SEC
DELTA 1128.39 KM
ATTN 18.0 DB
FIL 10.5 3.01



T-DELTA/8.5

1140 KM.

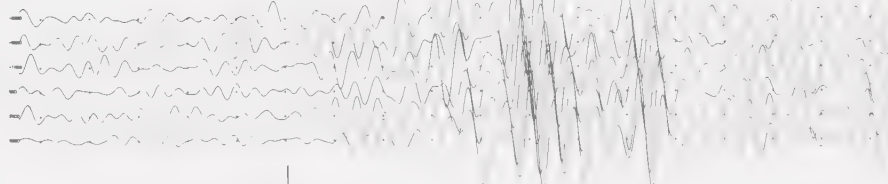
RECORD 1
MC 24.0 SHOT 9.0
TODIC 5.21 SEC
DELTA 1140.40 KM
ATTN 18.0 DB
FIL 10.5 3.0



T-DELTA/8.5

1232 KM.

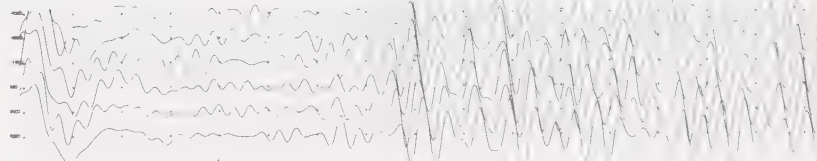
RECORD 5
MC 27.0 SHOT 6.0
TODIC 4.57 SEC
DELTA 1232.20 KM
ATTN 18.0 DB
FIL 0.5 3.01



T-DELTA/8.5

1428 KM.

RECORD 3
MC 31.0 SHOT 14.0
TODIC 4.25 SEC
DELTA 1428.43 KM
ATTN 18.0 DB
FIL 0.5 3.01



T-DELTA/8.5

1472 KM.

RECORD 15
MC 33.0 SHOT 16.0
TODIC 6.45 SEC
DELTA 1472.78 KM
ATTN 18.0 DB
FIL 0.5 3.01

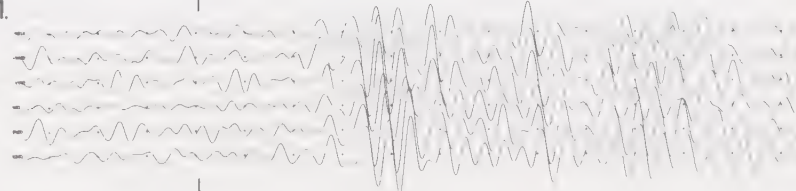


Figure 2.8 These same records after applying the
velocity filter.

136 137 138 139 140 141 142 143 144 145 146 147 148 149 150 151 152 153 154

VELOCITY
FILTER

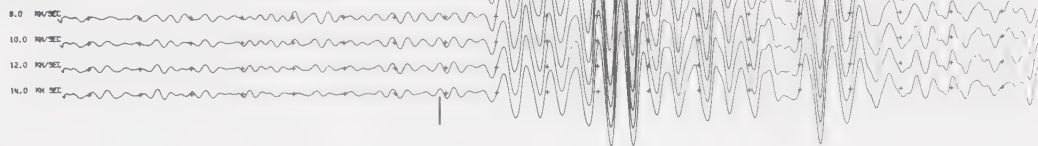
1128 KM.

10 S.

20 S.

RECORD 2 0 RT STRK

MC 38.0
SHFT 1.0
1.00 5.0 HZ

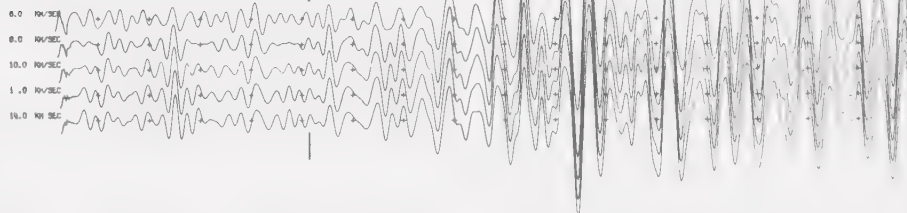


140 141 142 143 144 145 146 147 148 149 150 151 152 153 154

1140 KM.

RECORD 1 0 RT STRK

MC 24.0
SHFT 3.0
1.00 5.0 HZ

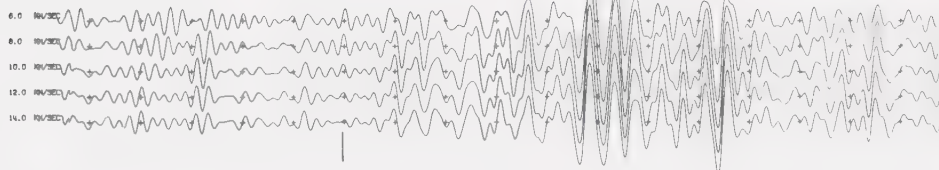


140 141 142 143 144 145 146 147 148 149 150 151 152 153 154

1232 KM

RECORD 5 0 RT STRK

MC 27.0
SHFT 8.0
1.00 5.0 HZ

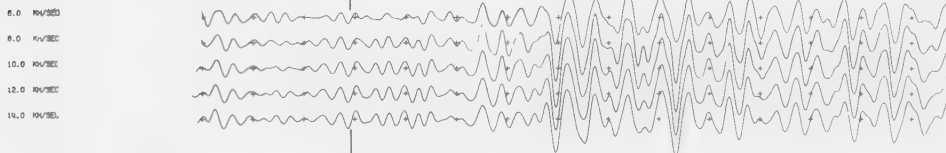


+ + + + + + + + + + + + + + + + +

1428 KM.

RECORD 3 0 RT STRK

MC 31.0
SHFT 14.0
1.00 5.0 HZ



0 181 182 183 184 185 186 187 188 189 190 191 192 193 194 195

1472 KM.

RECORD 15 0 RT STRK

MC 32.0
SHFT 15.0
1.00 5.0 HZ

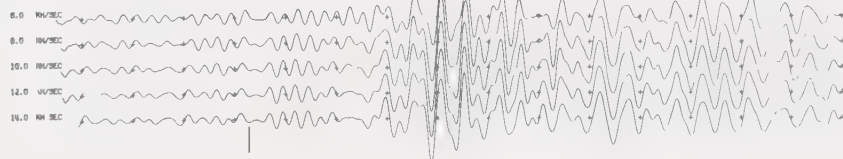


Figure 2.9 These same records after applying the
8th root stack filter.

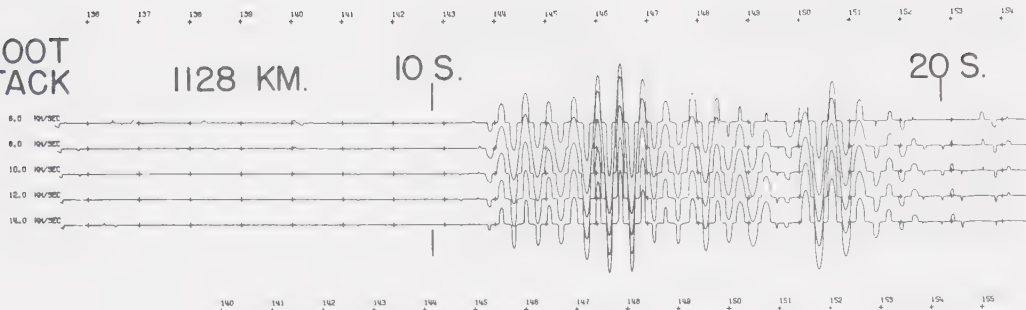
8 ROOT
STACK

1128 KM.

10 S.

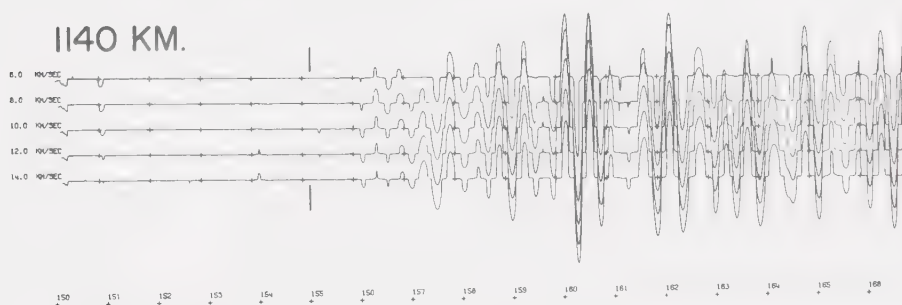
20 S.

RECORD 2 8 RT STACK
MC 25.0
0.50 3.0 HZ



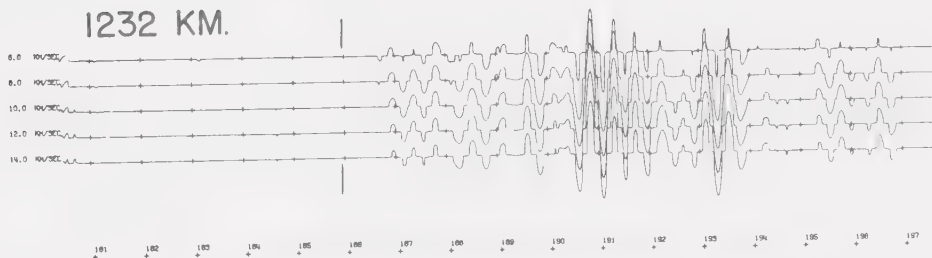
1140 KM.

RECORD 1 8 RT STACK
MC 24.0
0.50 3.0 HZ



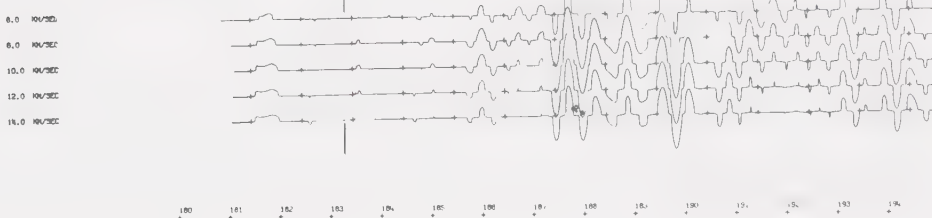
1232 KM.

RECORD 5 8 RT STACK
MC 27.0
0.50 3.0 HZ



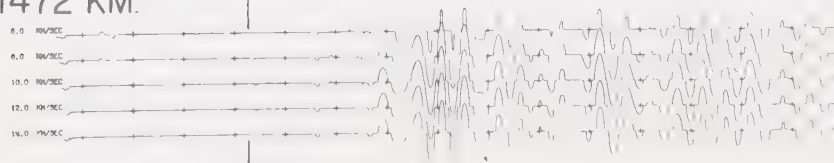
1428 KM.

RECORD 3 8 RT STACK
MC 31.0
0.50 3.0 HZ



1472 KM.

RECORD 15 8 RT STACK
MC 32.0
0.50 3.0 HZ



greater noise rejecting ability than the normal stack, and also had better velocity resolution. It achieves this at the expense of signal distortion, the rejection and distortion increasing as a function of N .

The outputs of the various stack routines were displayed using the CalComp 663 digital plotter. Here each output trace is the result of assuming different spread velocities. The sensitivity of the beamforming filter is limited by the long wavelegths (high velocity, low frequency) and the shortness of the spread. A geophone separation of one or two kilometers would have been more appropriate, as seen in retrospect. However, the results were satisfactory, as verified by the figures.

Let us consider the stacking procedures in more detail. Consider K channels of data,

$$X_j(t) \quad j = 1, K \quad 2.1$$

with channel j having gain G . Let the channels be sampled at m samples per second for T seconds, giving us a K by M matrix

$$X_{i,j} \quad i = 1, M ; \quad j = 1, K \quad 2.2$$

where M is the total number of samples per channel and is given by

$$M = T m \quad 2.3$$

and i is the time index. To bring all traces to a common gain G , let

$$X_{i,j} = (G/G_j) X_{i,j} \quad i = 1, M; \quad j = 1, K \quad 2.4$$

Let the distance of the j^{th} geophone from the center of the spread be D_j . Then, assuming a velocity V for the incoming wave, the lag τ_j of channel j in samples per second is given by

$$\tau_j = (D_j / V) m \quad 2.5$$

The resultant of the normal stack is given by

$$R_i = (1/C) \sum_{j=1}^K C_j X_{i+\tau_j, j} \quad 2.6$$

where

$$C = \sum_{j=1}^N C_j \quad 2.7$$

and C_j is the weighting coefficient of the j^{th} trace.

For the N^{th} root stack, the intermediate result is

$$B_{N,i} = \left(\frac{1}{C}\right) \sum_{j=1}^K C_j X_{i+\tau_{j,j}} \left| C_j X_{i+\tau_{j,j}} \right|^{\frac{1}{N+1}} \quad 2.8$$

and the final result is

$$R_{N,i} = B_{N,i} \left| B_{N,i} \right|^{N-1} \quad 2.9$$

This can be summed up as

$$R_{N,i} = \left[\left(\frac{1}{C}\right) \sum_{j=1}^K (C_j X_{i+\tau_{j,j}})^{1/N} \right]^N \quad 2.10$$

Note how the sign is conserved in the N^{th} root (equation 2.8) and the N^{th} power (equation 2.9) operations.

Let us consider the suppression of a spike of amplitude A at $i=I$ on channel J . Assuming all signals are the same except for phase, we have, letting $C_j=1$ for all j ,

$$R_i = \left(\frac{1}{K}\right) \sum_{j=1}^K X_{i-\tau_{j,j}} \quad 2.11$$

$$= \left(\frac{1}{K}\right) \sum_{\substack{j=1 \\ j \neq J}}^K S_i + S_i + A \delta_{i-I} \quad 2.12$$

where $\delta_i = \begin{cases} 0 & \text{if } i \neq 0 \\ 1 & \text{if } i = 0 \end{cases}$

and S_i is the common signal with the phase difference removed. Therefore

$$R_i = S_i + (1/K) A \delta_{i-I} \quad 2.13$$

The normal stack has reduced the amplitude of the spike by a factor of K , which is the number of traces. If the recorded signal consisted of a wanted signal and noise as represented by a Gaussian distribution of spikes, it can be shown that the signal to noise ratio is improved by a factor of $\frac{1}{2}\sqrt{K}$ (Smith, 1956).

Similarly, for the N^{th} root stack,

$$B_{N,i} = \left(\frac{1}{K}\right) \sum_{j=1}^K \left| x_{i-\tau_j,j} \right|^{1/N} \quad 2.14$$

$$= \left(\frac{1}{K}\right) \sum_{\substack{j=1 \\ j \neq J}}^K S_i^{1/N} + \left(S_i + A \delta_{i-I}\right)^{1/N} \quad 2.15$$

$$= \left(\frac{K-1}{K}\right) S_i^{1/N} + \left(\frac{1}{K}\right) \left(S_i + A \delta_{i-I}\right)^{1/N} \quad 2.16$$

If S_i is vanishingly small as compared to A , then a first order approximation can be used, giving us

$$S_i + A \doteq A \quad 2.17$$

Therefore

$$B_{N,i} \doteq S_i^{1/N} + (1/K) A^{1/N} \delta_{i-1} \quad 2.18$$

and

$$R_{N,i} \doteq \left(S_i^{1/N} + (1/K) A^{1/N} \delta_{i-1} \right)^N \quad 2.19$$

Using the same approximation

$$R_{N,i} \doteq S_i + (1/K)^N A \quad 2.20$$

Therefore spike rejection varies as K^{-N} . However, in using the crude approximation (equation 2.17), the filter operator was changed into a linear one, whereas, in fact, the filter is highly non-linear. A much more sophisticated treatment is necessary to gain any more than the general behaviour of these filters as presented here and in figure 2.10.

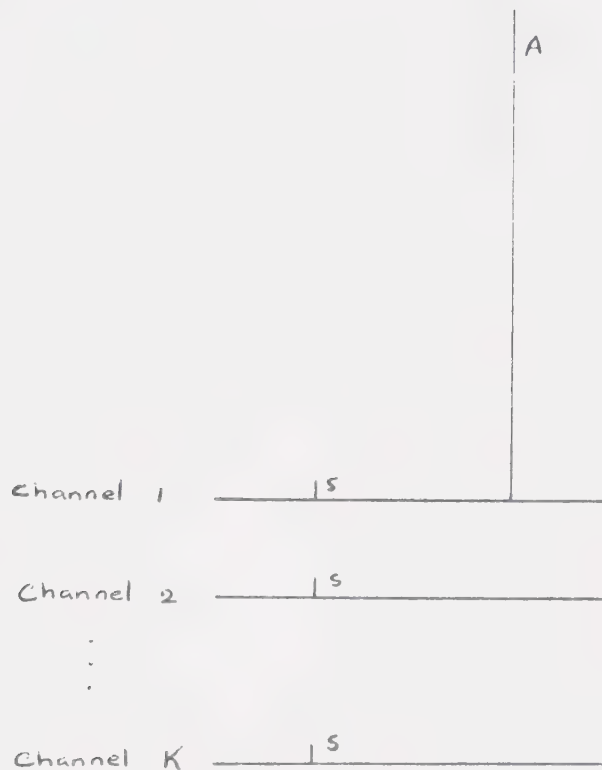
2.5 Display of Results

The display is just as important as the elimination of noise, because the organization of the display plays a major role in signal interpretation. All displays

Figure 2.10 Spike attenuation using the N^{th} root stack on K channels of input.

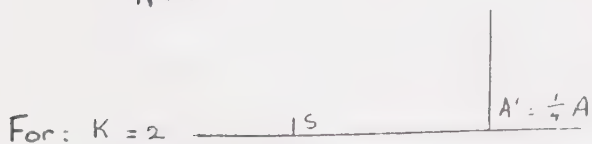
Nth ROOT STACK - ATTENUATION OF A SPIKE

INPUT: Signal of amplitude S
Spike of amplitude A

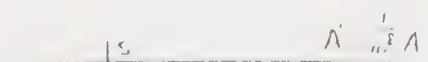
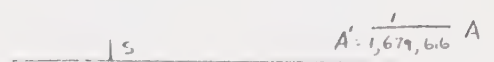
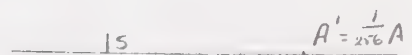


OUTPUT: Signal Amplitude $S' = S$
Spike Amplitude $A' = AK^{-N}$

$N=2$



$N=8$



were generated on the IBM 360/67 computer and plotted using a CalComp model 663 digital plotter. Even the unfiltered records could be improved by organizing the record display, so that the center axis of each trace was displaced from the time axis a distance proportional to the displacement of the corresponding geophone from the center of the spread; hence the apparent spread velocity could be read directly from the display. This proportional factor and the gain level could be adjusted to ensure that each trace was distinct from another and event character, frequency, and amplitude could readily be compared on all records. This was not necessarily the case with the field monitor records, particularly when the recording was made in the reverse mode; in this case the traces were scrambled, and it required the flexibility of the CalComp plotter to display these records in a meaningful manner.

Signal interpretation involves the identification and timing of events, which could not be done on the computer. An experienced observer, through a visual display, is able to perform complex and poorly understood (therefore unprogrammable) correlation functions to identify these events and trace them across the profile, provided that the signal to noise ratio is large enough. The enhancement techniques are used to unmask the signal from the noise, but cannot by themselves interpret the

data; hence the importance of the visual displays. They are the tools of the interpreter.

Figures 2.5 to 2.9 are characteristic of the displays of individual records. To give a picture of the entire profile, a reduced travel time composite plot (figures 2.11 and 2.12) was composed using the best recordings, which were band-pass filtered and stacked. These and similar displays of the other records were then used in analysing the data.

Figure 2.11 Composite plot of velocity filtered records.

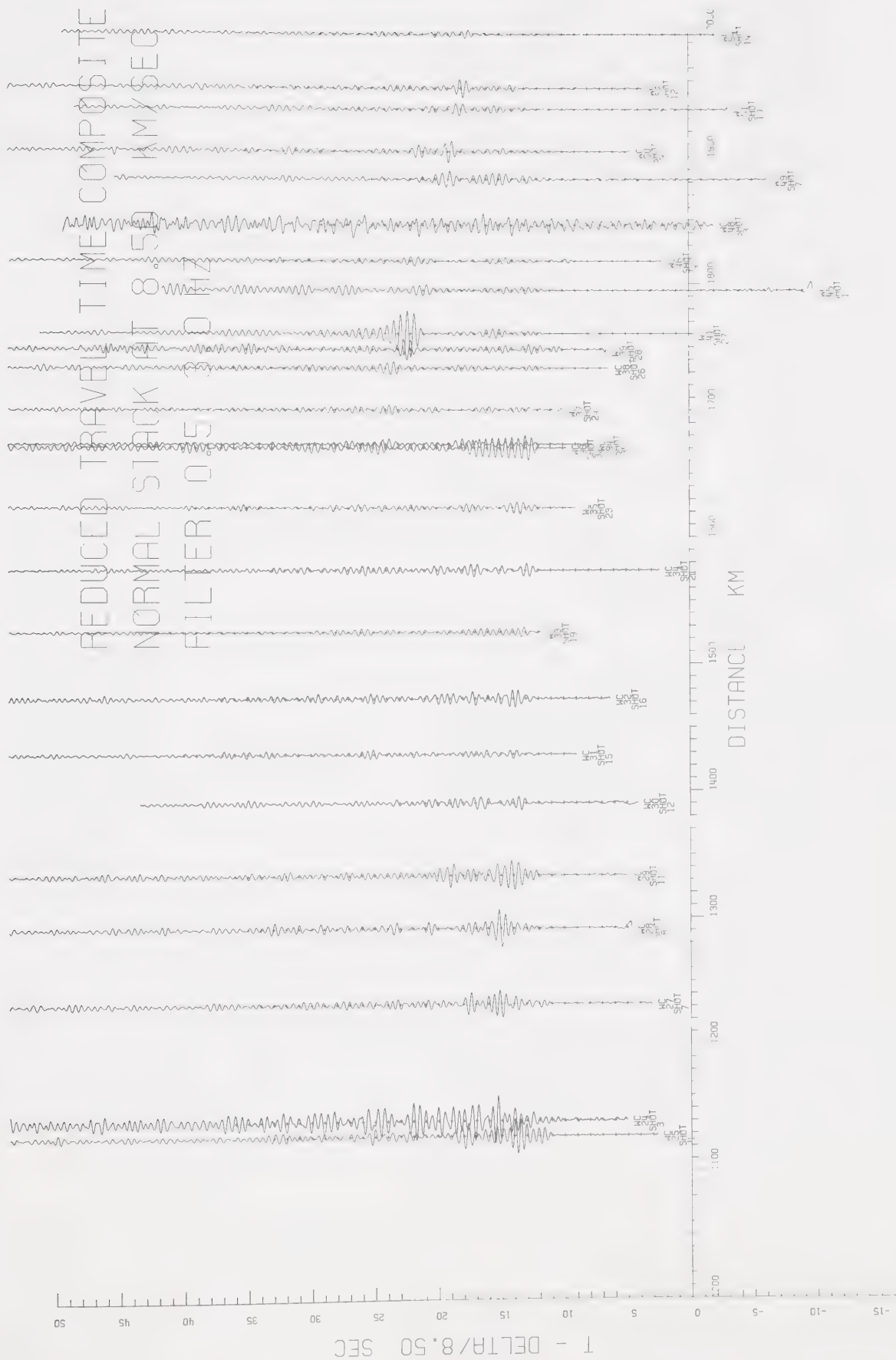
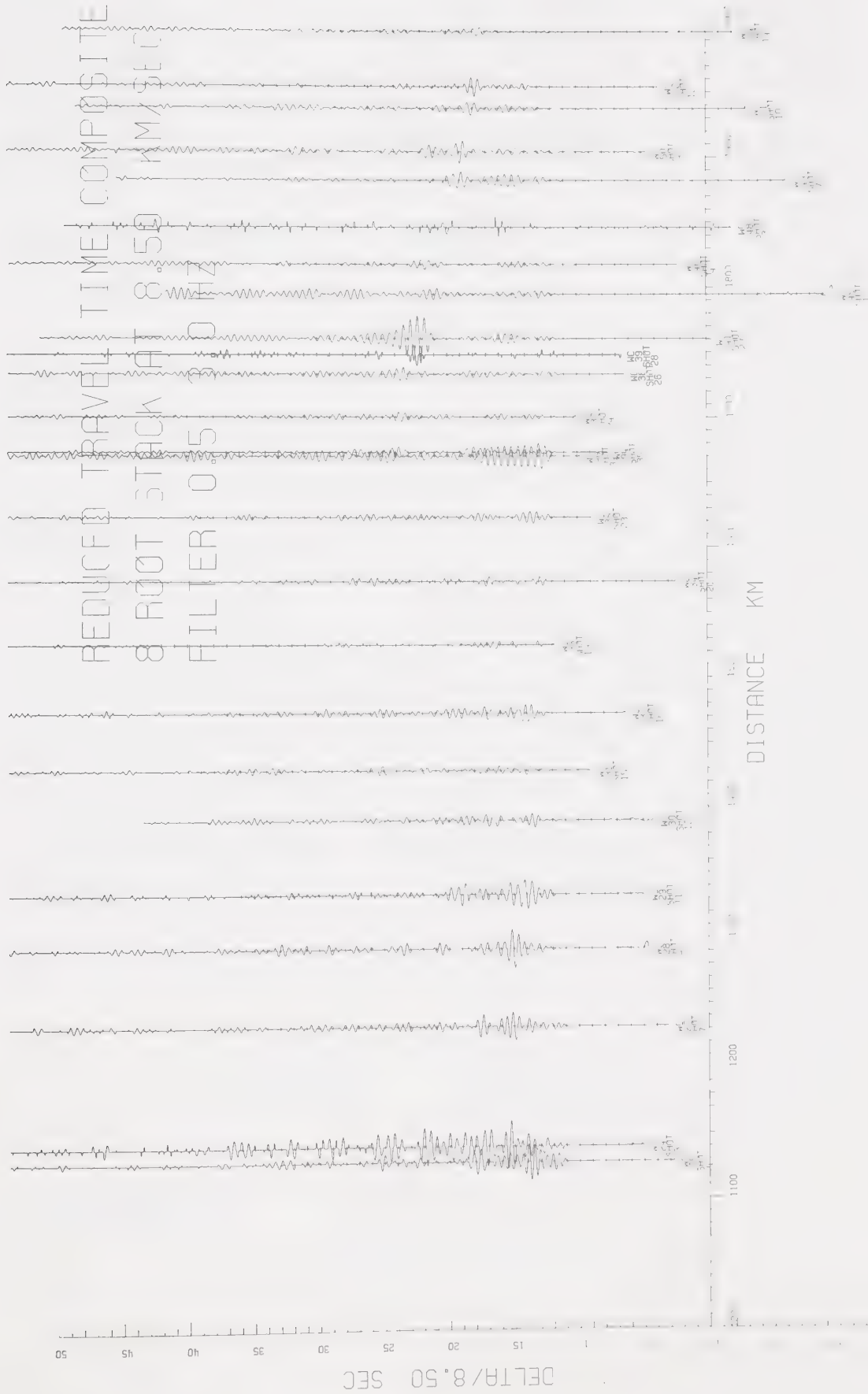


Figure 2.12 Composite plot of 8th root stack filtered records.



DELTA/8.50 SEC

DISTANCE KM

CHAPTER 3.

DATA INTERPRETATION

3.1 Earth Model - Ray Theory

Consider a radially symmetric earth made up of infinitesimally thin concentric homogeneous shells through which we shall pass a ray obeying Snell's law. Denote the physical properties of the i^{th} shell (between radii r_{i-1} and r_i) with the subscript i ; hence the angle of incidence and the angle of refraction at the i^{th} interface can be denoted as a_i and a'_{i+1} respectively, the angle being defined as the angle between the ray and the normal to the interface. Further, let the intersection of the interface and the ray be denoted as S_i (see figure 3.1). A given ray, then, can be defined by the angle of incidence at the source, a_s , at radius r_s or depth $r_0 - r_s$.

Snell's law states

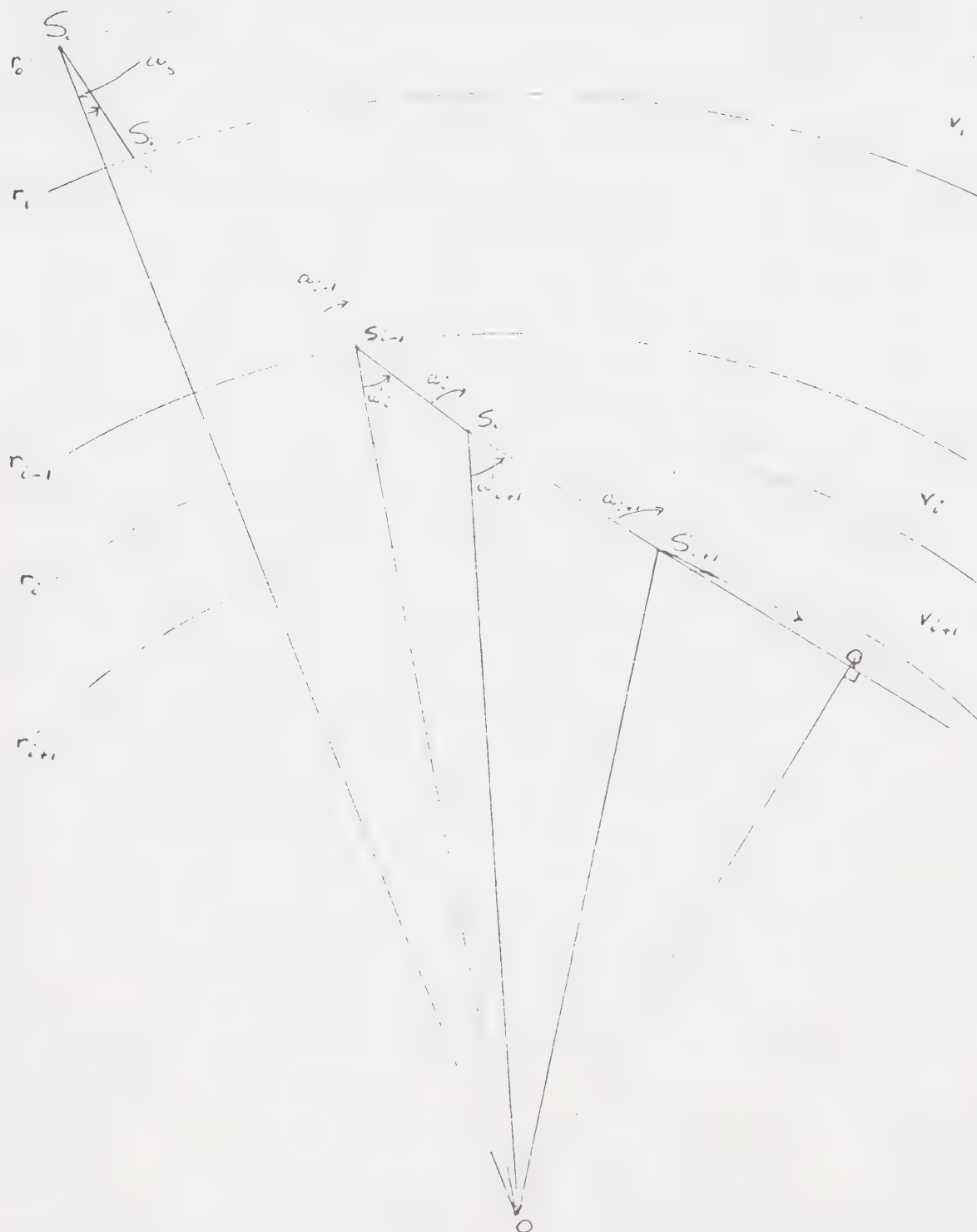
$$\frac{\sin a_i}{v_i} = \frac{\sin a'_{i+1}}{v_{i+1}} \quad 3.1$$

From geometry

$$r_i \sin a'_{i+1} = r_{i+1} \sin a_{i+1} \quad 3.2$$

Figure 3.1 Diagram of a ray passing through an earth
made up of homogeneous concentric shells.

RAY PASSING THROUGH A LAYERED EARTH



$$r_i \sin a'_{i+1} = QO \quad 3.3$$

where QO is the perpendicular distance from the ray segment in the i^{th} shell to the center of the earth (figure 3.1).

Therefore, Snell's law becomes

$$\frac{r_i \sin a_i}{v_i} = \frac{r_{i+1} \sin a_{i+1}}{v_{i+1}} \quad 3.4$$

$$= p \quad 3.5$$

where p is a constant known as the ray parameter, which is unique for each ray. Now we can drop the subscripts and consider the velocity function v as a continuous function of r ; that is, $v = v(r)$. Then the angle of incidence is also a continuous function of r , ($a = a(r)$), and the bottom of the ray, or the minimum radius of the ray, r_b , is defined by

$$a(r_b) = \pi/2 \quad 3.6$$

Hence the depth of deepest penetration may be defined as $r_0 - r_b$. Then

$$p = \frac{r \sin a(r)}{v(r)} \quad 3.7$$

$$p = \frac{r_s \sin a(r_s)}{v(r_s)} \quad 3.8$$

That is, the ray parameter is defined by the radius of the source and the angle of incidence at the source, and is a constant everywhere on the ray. Then by the bottom condition stated in equation 3.6

$$p = r_b / v(r_b) \quad 3.9$$

or

$$r_b = p v(r_b) \quad 3.10$$

Equation 3.10 is in the form of a **transcendental** equation which, depending on the function $v(r)$, may or may not be solved explicitly for r_b . In cases where it cannot be solved explicitly, it may be solved by iteration.

Consider the ray path S originating at the polar co-ordinates $(r_s, 0)$ and with an initial angle of incidence a_s . An element ds of the ray path can be expressed as

$$\overrightarrow{ds} = dr \overrightarrow{u_r} + r d\theta \overrightarrow{u_\theta} \quad 3.11$$

where u_r and u_θ are unit vectors in the r, θ directions

respectively. Two identities are immediately apparent and are needed in the following development.

$$(ds)^2 = (dr)^2 + r^2 (d\theta)^2 \quad 3.12$$

$$\sin a \, ds = r \, d\theta \quad 3.13$$

whence

$$ds = r \, d\theta / \sin a \quad 3.14$$

$$= r^2 \, d\theta / p r \quad 3.15$$

from the definition of p given in equation 3.7. Then substituting equation 3.15 into equation 3.12

$$(d\theta)^2 r^4 / p^2 r^2 = (dr)^2 + r^2 (d\theta)^2 \quad 3.16$$

$$d\theta = \pm \frac{p \, dr}{r \sqrt{(r/v)^2 - p^2}} \quad 3.17$$

Therefore the angular component of the ray path from its source to its depth of deepest penetration is given by

$$\theta_{sb} = p \int_{r_s}^{r_b} \frac{-dr}{r \sqrt{(r/v)^2 - p^2}} \quad 3.18$$

Solving for $d\theta$ in equation 3.13, substituting it into equation 3.12, and using equation 3.7 to eliminate $a(r)$, we get

$$(ds)^2 = (dr)^2 + r^2 (ds \sin a/r)^2 \quad 3.19$$

$$= (dr)^2 + r^2 (ds \, p/r)^2 \quad 3.20$$

$$= (dr)^2 + (p/r)^2 (ds)^2 \quad 3.21$$

or

$$ds = \pm \frac{dr}{\sqrt{1 - (p/r)^2}} \quad 3.22$$

$$= \pm \frac{r \, dr}{r^2 \sqrt{(r/r)^2 - p^2}} \quad 3.23$$

The time dt taken to traverse the path length ds is given by

$$dt = ds/v \quad 3.24$$

or

$$dt = \pm \frac{r \, dr}{v^2 \sqrt{(r/v)^2 - p^2}} \quad 3.25$$

Therefore the time taken to traverse the ray path from the source to the depth of deepest penetration is given by

$$T_{sb} = \int_{r_s}^{r_b} \frac{-r dr}{v^2 \sqrt{(r/v)^2 - p^2}} \quad 3.26$$

which can be denoted in the form

$$T_{sb} = \int_{r_s}^{r_b} f_T(r) dr \quad 3.27$$

and

$$O_{sb} = \int_{r_s}^{r_b} f_O(r) dr \quad 3.28$$

For a complete ray path, from source to receiver,

$$T_{sr} = \int_{r_s}^{r_b} f_T(r) dr - \int_{r_b}^{r_r} f_T(r) dr \quad 3.29$$

$$O_{sr} = \int_{r_s}^{r_b} f_O(r) dr - \int_{r_b}^{r_r} f_O(r) dr \quad 3.30$$

where r_r is the radius of the receiver. When $r_s = r_r$, this simplifies to the form

$$T_{sr} = 2 \int_{r_s}^{r_b} f_T(r) dr \quad 3.31$$

$$\theta_{sb} = 2 \int_{r_s}^{r_b} f_\theta(r) dr \quad 3.32$$

The equations of θ and T in the forms of equations 3.29 and 3.30 are the most useful, since different velocity functions may be used at different angular displacements from the source. That is, $v(r)$ can be varied as a function of θ and becomes $v(r, \theta)$. However, unless the ray parameter p is also varied, it is still assumed that the shells are radially symmetrical, but that the radius of the shell can be made to vary with θ for individual ray paths. In other words, the "dip" of the shell has not been taken into account unless the ray parameter p is suitably varied. Hence the usefulness of equations 3.29 and 3.30 is limited to varying the elevation and crustal structure under the source and the receiver, still assuming beds parallel to the surface of the earth. This can be accomplished by using the source velocity function in the down integral (r_s to r_b) and using a suitable velocity function in the up integral as based on the expected angular displacement from the source to the receiver end of the ray, as estimated by $2\theta_{sb}$ from equation 3.32. It should be possible to consider an asymmetric earth by varying the ray parameter p as

a function of the dip of the velocity shells as represented by spherical shells displaced from the center of the earth.

3.2 Solutions of the Ray Path Integrals

Note that both θ and T are of the form

$$X = \int_A^B f(x) dx \quad 3.33$$

There are several ways of evaluating this integral.

The obvious method is to evaluate

$$F(x) = \int f(x) dx \quad 3.34$$

and then

$$X = F(B) - F(A) \quad 3.35$$

However, $f(x)$, or rather $f_\theta(r)$ and $f_T(r)$, are not well known functions, as $v(r)$ is assumed at discrete values of r , and some form of extrapolation is used between these points. Therefore $v(r)$ is, at best, a continuous function with discontinuous high order derivatives. Also, integral solutions exist for only a limited number of

velocity functions, and these may not necessarily be physically realistic.

Let us consider a finite number of concentric homogeneous shells. When $v(r) = v_i$, a constant, for $r_{i-1} \leq r < r_i$, then within this interval equation 3.18 becomes

$$\theta_{i,i-1} = p \int_{r_i}^{r_{i-1}} \frac{-dr}{r \sqrt{(r/v_i)^2 - p^2}} \quad 3.36$$

$$= p v_i \int_{r_i}^{r_{i-1}} \frac{-dr}{r \sqrt{r^2 - p^2 v_i^2}} \quad 3.37$$

$$= \cos^{-1} \left(\frac{p v_i}{r_i} \right) - \cos^{-1} \left(\frac{p v_i}{r_{i-1}} \right) \quad 3.38$$

Let I be an integer such that $r_{I-1} < r_b \leq r_I$ and note that $r_b \geq p v_I$. The equality holds for the refraction and the inequality for the reflection of the ray from the I^{th} interface. Hence, for refraction,

$$\cos^{-1} (p v_I / r_b) = \cos^{-1} (1) \quad 3.39$$

$$= 0 \quad 3.40$$

and must be set to zero, since a small round off error could result in an argument greater than 1 and hence an

imaginary angle. Therefore

$$\begin{aligned} \theta_{sb} = & \sum_{i=1}^{I-1} \cos^{-1} \left(\frac{p v_i}{r_i} \right) - \cos^{-1} \left(\frac{p v_{i-1}}{r_{i-1}} \right) \\ & + \cos^{-1} \left(\frac{p v_I}{r_{I-1}} \right) - \cos^{-1} \left(\frac{p v_I}{r_b} \right) \end{aligned} \quad 3.41$$

and

$$\begin{aligned} \theta_{br} = & -\cos^{-1} \left(\frac{p v'_J}{r_b} \right) + \cos^{-1} \left(\frac{p v'_J}{r_{J-1}} \right) \\ & + \sum_{j=J-1}^1 \cos^{-1} \left(\frac{p v'_j}{r_j} \right) - \cos^{-1} \left(\frac{p v'_j}{r_{j-1}} \right) \end{aligned} \quad 3.42$$

where v'_j may be a new velocity step function and J is an integer such that $r_{J-1} < r'_b \leq r_J$ and $r_b \geq p v'_J$.

If $r'_b \neq r_b$, then the bottom of the ray is in the region where $v = v(r, \theta)$ and the ray parameter must be adjusted from the old value p to p' such that either

i) in the case of reflection from the I^{th} interface

$$\sin^{-1} (p v_I / r_b) = \sin^{-1} (p' v'_J / r_b) \quad 3.43$$

or

$$p' = p v_I / v'_J \quad 3.44$$

which is derived from the requirement that the angle of

incidence be equal to the angle of reflection, still assuming concentric shells, or

ii) in the case of refraction

$$p' = r_b / v_J' \quad 3.45$$

$$= p v_I / v_J' \quad 3.46$$

which follows from the requirement that the ray be travelling tangential to the curve of $r = r_b$. This can be considered as a special case of reflection where the angle of incidence is $\pi/2$.

Let us consider the solution to the travel time.

$$T_{i,i-1} = - \int_{r_i}^{r_{i-1}} \frac{r \, dr}{v_i \sqrt{r^2 - p^2 v_i^2}} \quad 3.47$$

$$= - \frac{1}{v_i} \int_{r_i}^{r_{i-1}} \frac{r \, dr}{\sqrt{r^2 - p^2 v_i^2}} \quad 3.48$$

$$= \frac{\sqrt{r_i^2 - p^2 v_i^2}}{v_i} - \frac{\sqrt{r_{i-1}^2 - p^2 v_i^2}}{v_i} \quad 3.49$$

and

$$T_{sb} = \sum_{i=1}^{I-1} \frac{\sqrt{r_i^2 - p^2 v_i^2}}{v_i} \frac{-\sqrt{r_{i-1}^2 - p^2 v_i^2}}{v_i} + \frac{\sqrt{r_{I-1}^2 - p^2 v_I^2}}{v_I} \frac{-\sqrt{r_b^2 - p^2 v_I^2}}{v_I} \quad 3.50$$

and

$$T_{br} = \frac{-\sqrt{r_b^2 - p'^2 v_J'^2}}{v_J'} + \frac{\sqrt{r_{J-1}^2 - p'^2 v_J'^2}}{v_J'} + \sum_{j=J-1}^1 \frac{\sqrt{r_j^2 - p'^2 v_j'^2}}{v_j'} \frac{-\sqrt{r_{j-1}^2 - p'^2 v_j'^2}}{v_j'} \quad 3.51$$

Again note that in the case of refraction $r_b = p v_I$ and the calculation of the bottom term must be set to zero, since a small error could result in an imaginary square root.

A solution for θ exists when a continuous velocity distribution of the form

$$v_i(r) = \alpha_i + \beta_i r \quad 3.52$$

is assumed between the shell radii r_{i-1} and r_i . Then

$$\theta_{i,i-1} = -p \int_{r_i}^{r_{i-1}} \frac{v_i dr}{r \sqrt{r^2 - p^2 v_i^2}} \quad 3.53$$

$$\theta_{i,i-1} = -p \int_{r_i}^{r_{i-1}} \frac{(\alpha_i/r + \beta_i) dr}{\sqrt{(1-p^2\beta_i^2)r^2 - 2p^2\alpha_i\beta_i r - \alpha_i^2 p^2}} \quad 3.54$$

Let

$$a_i = -p^2 \alpha_i^2 \quad 3.55$$

$$b_i = -2p^2 \alpha_i \beta_i \quad 3.56$$

$$c_i = 1 - p^2 \beta_i^2 \quad 3.57$$

and

$$R_i(r) = a_i + b_i r + c_i r^2 \quad 3.58$$

Then

$$b_i^2 - 4a_i c_i = 4p^2 \alpha_i^2 \quad 3.59$$

Whence

$$\begin{aligned} \theta_{i,i-1} &= p\alpha_i \int_{r_i}^{r_{i-1}} \frac{(r) dr}{\sqrt{R_i}(r)} \\ &\quad + p\beta_i \int_{r_i}^{r_{i-1}} \frac{(r) dr}{\sqrt{R_i}} \end{aligned} \quad 3.60$$

Let $\theta'_{i,i-1}$, $\theta''_{i,i-1}$ represent the first and second terms respectively. Since $a < 0$ for all p , α_i , then

$$\begin{aligned} \theta'_{i,i-1} &= \sin^{-1} \left(\frac{-p\beta_i r_{i-1} + p\alpha_i}{r_{i-1}} \right) \\ &\quad - \sin^{-1} \left(\frac{-p\beta_i r_i + p\alpha_i}{r_i} \right) \end{aligned} \quad 3.61$$

For $c < 0$,

$$\begin{aligned} \theta''_{i,i-1} &= \frac{p\beta_i}{\sqrt{p^2\beta_i^2 - 1}} \left[\sin^{-1} \left(\frac{(p^2\beta_i^2 - 1)r_{i-1} + p^2\alpha_i\beta_i}{p\alpha_i} \right) \right. \\ &\quad \left. - \sin^{-1} \left(\frac{(p^2\beta_i^2 - 1)r_i + p^2\alpha_i\beta_i}{p\alpha_i} \right) \right] \end{aligned} \quad 3.62$$

and for $c > 0$,

$$\begin{aligned} \theta''_{i,i-1} &= \frac{p\beta_i}{\sqrt{c_i}} \ln \left[\sqrt{R_i}(r_{i-1}) + r_{i-1}\sqrt{c_i} + \frac{b_i}{2\sqrt{c_i}} \right] \\ &\quad - \frac{p\beta_i}{\sqrt{c_i}} \ln \left[r_i\sqrt{R_i} + r_i\sqrt{c_i} + \frac{b_i}{2\sqrt{c_i}} \right] \end{aligned} \quad 3.63$$

Therefore

$$\theta_{sb} = \sum_{i=1}^{I-1} \theta'_{i-1,i} + \theta''_{i-1,i} + \theta'_{I-1,I^*} + \theta''_{I-1,I^*} \quad 3.64$$

where we define $r_{I^*} = r_b$ and $r_{i-1} < r_b \leq r_I$.

Similarly, on changing the velocity function, we obtain

$$\theta_{br} = \theta'_{J-1, J^*} + \theta''_{J-1, J^*} + \sum_{j=J-1}^1 \theta'_{j-1, j} + \theta''_{j-1, j} \quad 3.65$$

where again the p parameter is reset to

$$p' = r_b / v'(r_b) \quad 3.66$$

The equivalent integral for time using $v = \alpha + \beta r$ cannot be readily integrated, and no solution has been derived here.

As expressed in equations 3.18 and 3.26, both θ and T are of the form $X = \int_a^b f(x)dx$. When the function $v(r)$ is not well known and various methods of extrapolation between radii of assumed velocities are used, then a center point integration formula of the form

$$X = \sum_{i=0}^N f(x_{ci}) \Delta x \quad 3.67$$

$$= (B-A) \sum_{i=0}^N f(x_{ci}) \quad 3.68$$

may be used, where N is an arbitrary positive integer and

$$\Delta x = (B-A) / N \quad 3.69$$

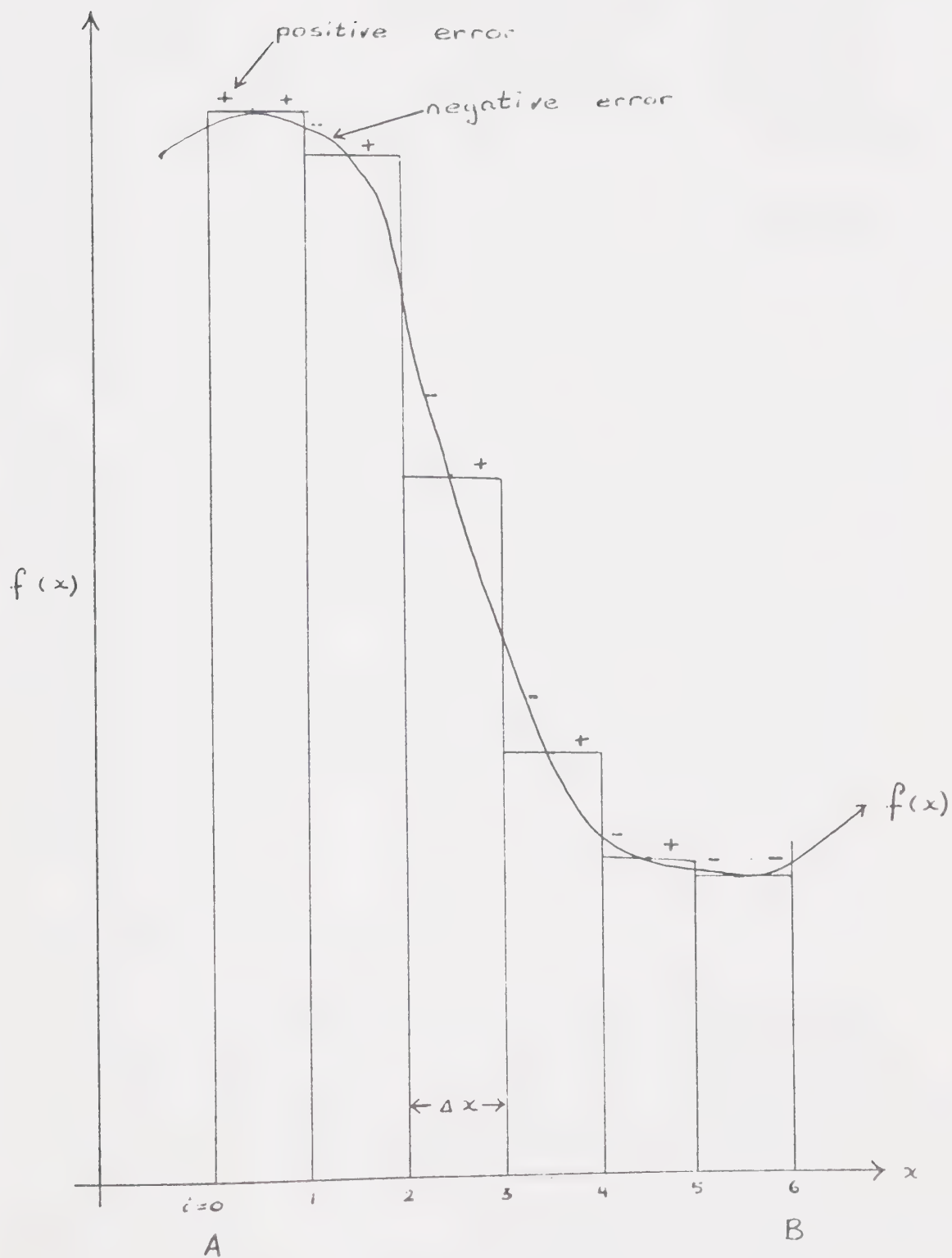
$$x_{ci} = \frac{1}{2} (x_i + x_{i+1}) \quad 3.70$$

$$x_i = A + i \Delta x \quad 3.71$$

Using this method, the integration of $f(x)$ is equated to the area under the curve $f(x)$, and this is approximated by the sum of the areas of several rectangles of height $f(x_i)$; $i = 0, N$ and of width Δx . Both positive and negative errors occur which tend to cancel each other (see figure 3.2), and which are further reduced by decreasing Δx . The accuracy is then limited by the accumulated round off errors, which increase as N is increased and hence as Δx is decreased.

With a knowledge of the behaviour of the function $f(x)$, it is possible to vary the size of Δx for different ranges of x . In our case, we are integrating down to a pole, the pole being the radius at which the ray bottoms. Far from the pole relatively large steps may be taken with small sacrifice to the accuracy of the approximation and with a large decrease in the accumulated round off error. As the pole is approached, the curvature of the function increases. Hence, smaller steps are used, and the error of the approximation is reduced. Also, the round off error is small, because each of the terms representing the area under the curve is of small width but of large height, therefore of considerable area. Another range of x exists, where the function is of considerable height and increasing rapidly. This occurs

Figure 3.2 Center point integration formula approximation
to the area under the curve.



CENTER POINT INTEGRATION APPROXIMATION

when the pole exists just below a low velocity shell, in which case there is a region immediately above this shell where finer increments in the integration are required. Thus by suitably varying Δx , it is possible to minimize both the error of the approximation and of the round off.

Fortran programs were written (see appendix) using both the thin shell constant velocity and the center point integration formulae. To check the accuracy of the programs, they were used to reproduce the travel times of Jeffreys and Bullen(1958); Lewis and Meyer (1967); Johnson (1967); and Herrin, Tucker, Taggart, Gordon, and Lobdell (1968). Furthermore, the two methods closely agreed with one another in each of the above checks. In addition, the center point integration formula agreed closely with the exact solution of the constant velocity formula in the case of a homogeneous earth.

3.3 Ray Flux Calculations

In conjunction with the travel time curves, ray paths and amplitude predictions were made. The ray paths were calculated by evaluating r, θ in each step of the integral and the results were plotted using the CalComp digital plotter. The energy density was calculated from the ray flux, which was shown by Bullen (1963) to be

$$E(\theta) = \frac{I \sin a_s}{r_r^2 \sin \theta \sin a_r} \left| \frac{da_s}{d\theta} \right| \quad 3.72$$

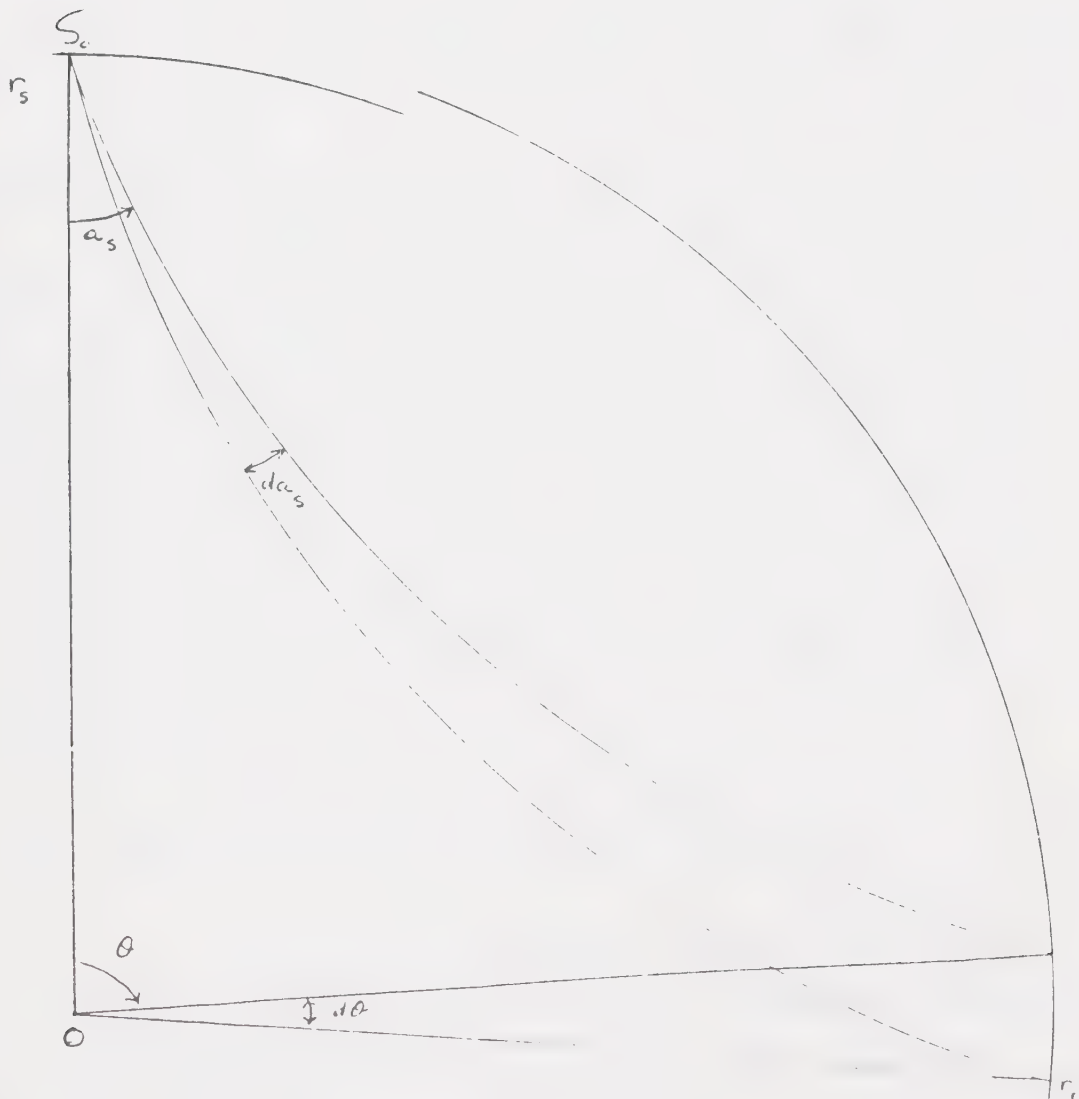
where I is a constant of proportionality denoting the energy per solid angle emitted by the source, a_s is the angle of incidence at the source, a_r is the angle of emergence at the receiver, r_r is the radius of the receiver, θ is the angular distance from source to receiver, and da_s , $d\theta$ are increments in a_s , θ respectively. To derive this equation we consider all the rays leaving the source between the angles of incidence a_s and $a_s + da_s$ (see figure 3.3). The energy radiated in this ray bundle is $2\pi I \sin a_s |da_s|$, the modulus of da_s being used to insure that this term is positive. This ray bundle arrives at the receiver radius r_r between the distances θ and $\theta + d\theta$, which sweeps out an area on a sphere of radius r_r given by $2\pi r_r^2 \sin \theta |d\theta|$. Again, the modulus of $d\theta$ is used, as $d\theta$ may be negative, whereas the area is always positive. Then the cross-sectional area of the ray bundle is given by $2\pi r_r^2 \sin \theta \cos a_r |d\theta|$ and the energy density at the angular distance θ is

$$E(\theta) = \frac{2\pi I \sin a_s |da_s|}{2\pi r_r^2 \sin \theta \cos a_r |d\theta|} \quad 3.73$$

$$= \frac{I \sin a_s}{r_r^2 \sin \theta \cos a_r} \left| \frac{da_s}{d\theta} \right| \quad 3.74$$

Figure 3.3 Diagram of two rays passing through the earth, showing the change in the angular displacement of the emerging ray for a small change in the angle of incidence.

DIVERGENCE OF A RAY BUNDLE



Finally, the square of the amplitude is proportional to the energy density, whereby

$$A(\theta) = I_1 \sqrt{E(\theta)} \quad 3.75$$

$$= I_1 \sqrt{\frac{I \sin a_s}{r_r^2 \sin \theta \cos a_r} \left| \frac{da_s}{d\theta} \right|} \quad 3.76$$

$$= \frac{I_2}{r_r} \sqrt{\frac{\sin a_s}{\sin \theta \cos a_r} \left| \frac{da_s}{d\theta} \right|} \quad 3.77$$

Using angles of incidence a_s , $a_s + da_s$, and $a_s - da_s$, rays were passed, which arrived at the receiver radius with an angular distance of θ_r , θ_{r+} , and θ_{r-} respectively. Hence $d\theta$ could be estimated using the first difference method on either side of a_s and smoothed by taking the average of these terms. Thus all the arguments of equation 3.77 are known and $A(\theta)$, along with the travel time curve, can be calculated for any given velocity distribution.

3.4 Interpretation of the Travel Time Curve

The various earth models were derived by varying the velocity function until a good fit was made between the theoretical travel time curves and the events picked from the records. Model U of A #1 was fit to the first arrivals and to a prominent secondary

arrival as reported in the Technical Letter #6 (Warren et al., 1967). The ray and travel time diagrams are shown in figures 3.4 and 3.5, the latter also showing the Lewis and Meyer (1967) model for comparison. The Lewis and Meyer profile was also a part of Project Early Rise and was run along the 49th parallel (see figure 1.1), which is close to the Western Canada profile. Therefore, the two profiles should show similar results, as in fact they do, as illustrated in the diagram.

When a full analysis of the secondary arrivals had been made, it became evident that a simple model such as a modification of U of A #1 could not explain all of the arrivals. In order to explain the shadow zone and cusping in the travel time curve, one needs velocity reversals and large velocity gradients. Model U of A #3 produced the best fit to the observed data (figures 3.4 and 3.6). This model is markedly different from U of A #1. By removing the sharp corners of the velocity function of U of A #3, a modification, U of A #3a, resulted. As seen in figure 3.6, there was no significant difference in the resulting travel time curves of these two models. When the ray criterion of explaining events was relaxed, and the possibility of diffraction was used to explain the extreme ends of the cusps, then U of A #2 produced the best fit to all parts of the travel time curve

Figure 3.4 Ray diagram for body waves passing through earth models U of A #1 and U of A #3.

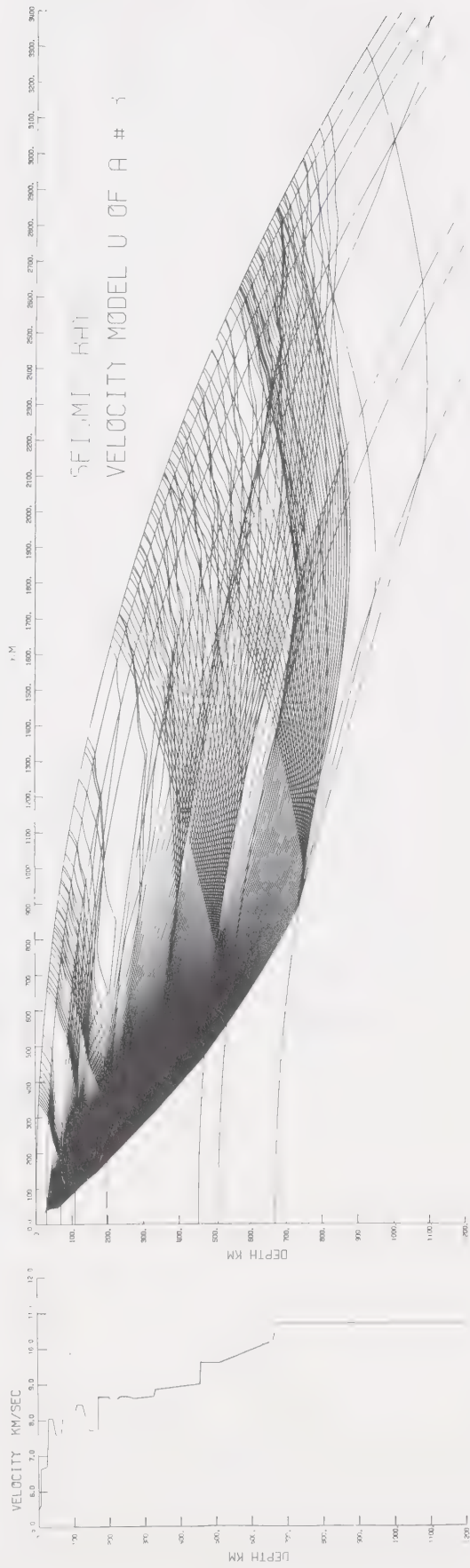
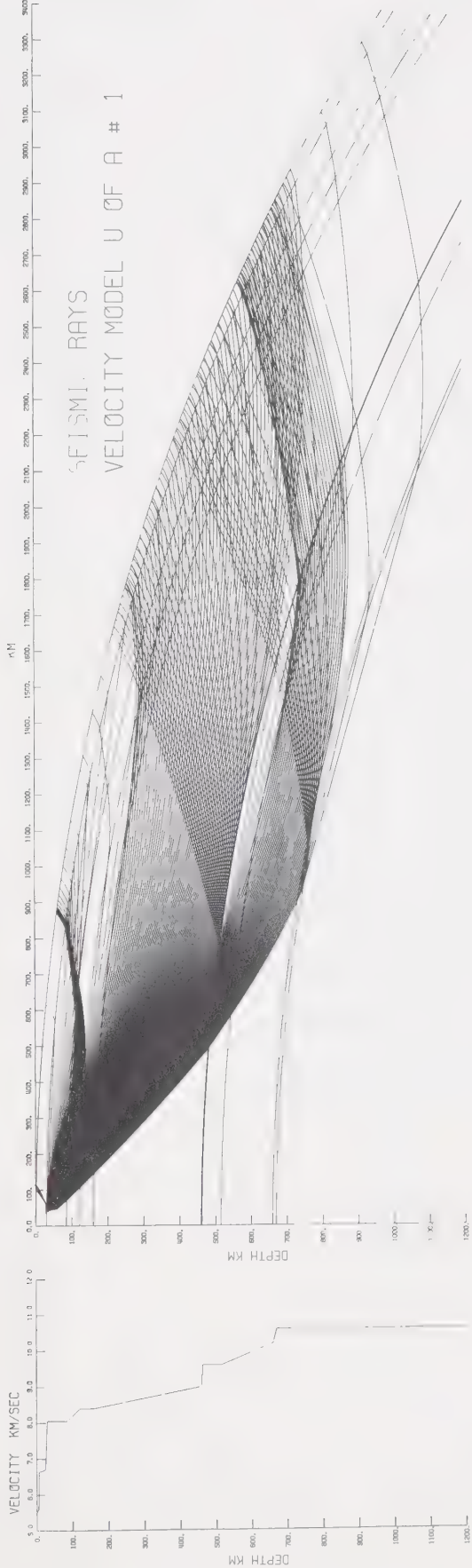


Figure 3.5 Velocity and travel time curves of the Lewis and Meyer model and the University of Alberta model U of A #1. Also shown are the observations of the first events and a prominent secondary event of the Western Canada profile.

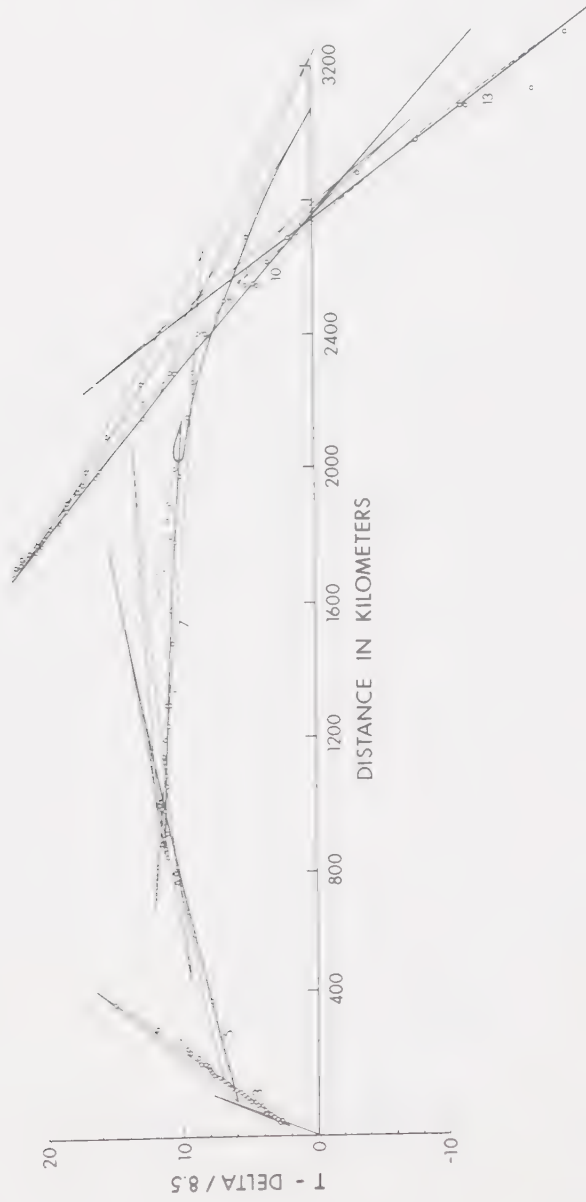
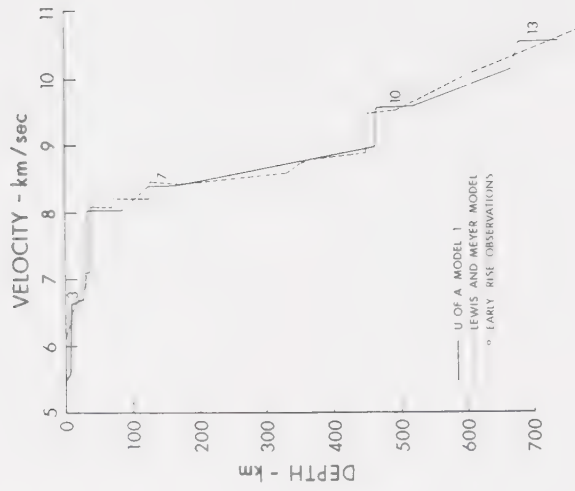
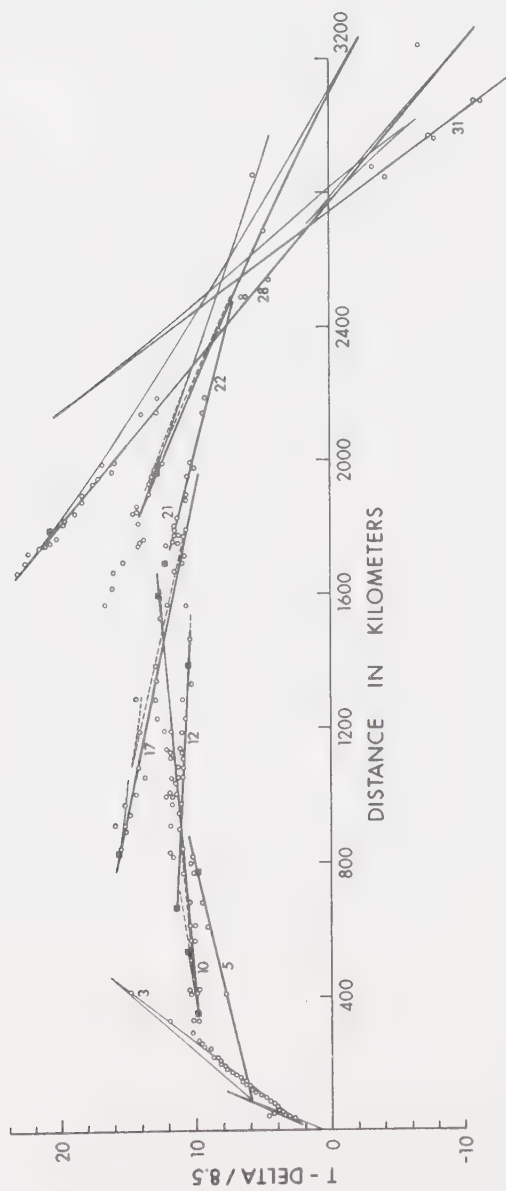
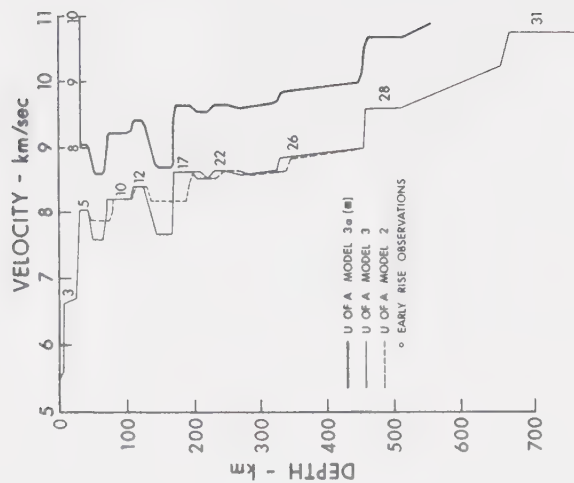


Figure 3.6 Velocity and travel time curves of the models U of A #2, U of A #3, and U of A #3a along with the Western Canada profile observations.



except the tips of the cusps, as shown by figures 3.6 and 3.7. The selection of a unique model to fit the data and possibly the determination of the shape of the transition zones lies in the matching the predicted amplitudes to the observed ones, as well as maintaining the fit to the observed travel time curve. This work is presently in progress.

Figure 3.8 is presented to summarize this work. It shows U of A #3, which is a model fitting a continental profile, and compares it to a model worked out by Johnson(1967), which is based on an oceanic profile. Also, a model based on a summary of the United States continental data (Herrin et al., 1968) is shown for further comparison. The rough features of our model and that of Johnson are seen to coincide, with ours showing a delay of about 2 seconds. The Herrin model lies slightly above model U of A #3 and has none of the detailed cusping of our model. Further work in this area should clarify the details of the upper mantle, but the gross features must be as represented here. In particular, a reversal of this profile should clarify the true velocities of the various zones.

Figure 3.7 Ray diagram for body waves passing through the earth model U of A #2.

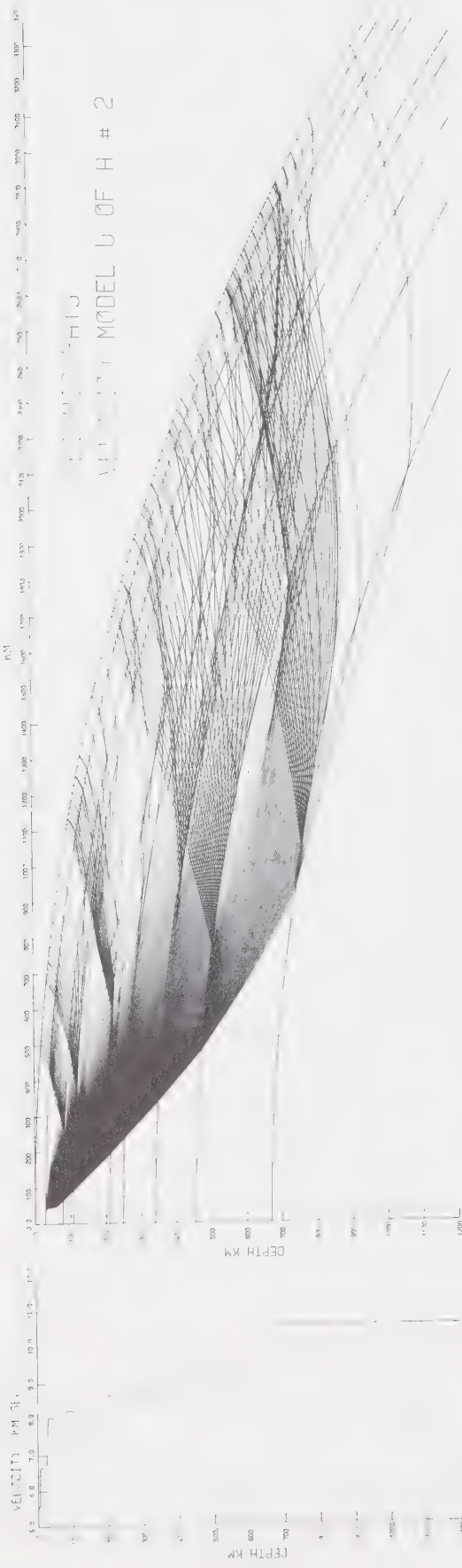
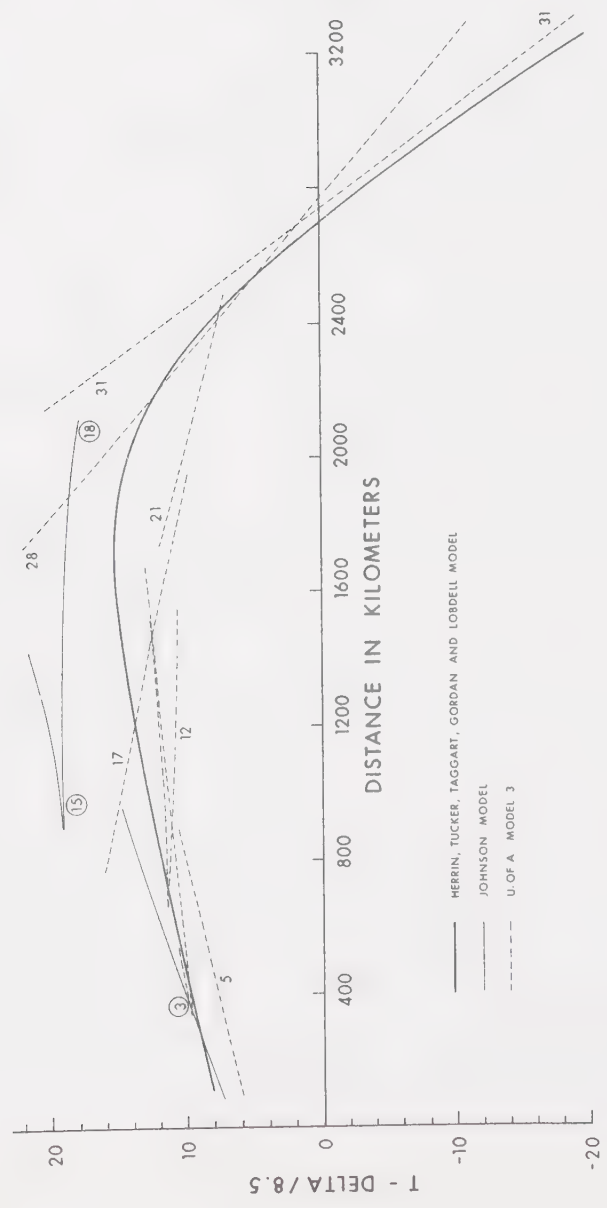
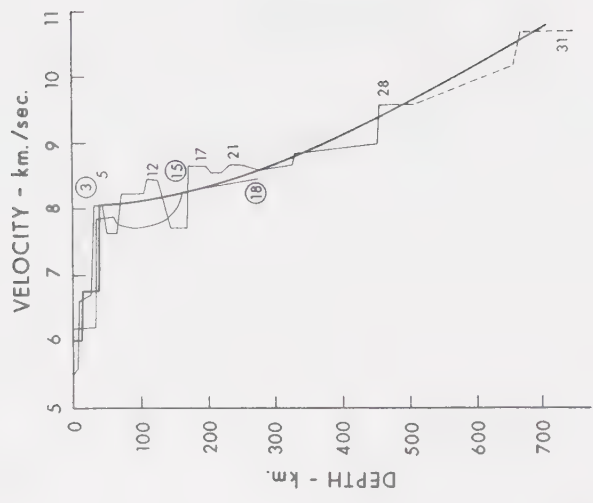


Figure 3.8 Velocity and travel time curves of the final model produced by the University of Alberta (U of A #3) along with those resulting from the oceanic model produced by Johnson and the average crustal model produced by Herrin, Tucker, Taggart, Gordon, and Lobdell.



BIBLIOGRAPHY

- Alpaslan, Tümer. "Spectral Behaviour of Short Period Body Waves and the Synthesis of Crustal Structure in Western Canada", M.Sc. Thesis, University of Alberta, November 1968.
- Berry, M. J., and G. F. West. "An Interpretation of the First - Arrival Data of the Lake Superior Experiment by the Time - Term Method", Bulletin of the Seismological Society of America, 56 #1 (February 1966), 141 - 171.
- Bullen, K. E. An Introduction to the Theory of Seismology. 3rd edition. Cambridge, 1963.
- Cumming, G. L., and E. R. Kanasewich. "Seismic Arrivals from the Earth's Upper Mantle", Nature, 206 #4981 (April 1965), 248 - 249.
- Clowes, Ronald Martin. "Deep Crustal Seismic Reflections at Near - Vertical Incidence", M.Sc. Thesis, University of Alberta, May 1966.
- Clowes, Ronald Martin. "Seismic Reflection Investigation of Crustal Structure in Southern Alberta", Ph.D. Thesis, University of Alberta, August 1969.

- Herrin, Eugene, William Tucker, James Taggart, David W. Gordon, and John L. Lobdell. "Estimation of Surface Focus P Travel Times", Bulletin of the Seismological Society of America, 58 #4 (August 1968), 1273 - 1291.
- Jeffreys, Harold, and K. E. Bullen. Seismological Tables. London, 1958.
- Johnson, Lane R. "Array Measurements of P Velocities in the Upper Mantle", Journal of Geophysical Research, 72 #24 (December 1967), 6309 - 6325.
- Lewis, Brian T. R., and Robert P. Meyer. "A Seismic Investigation of the Upper Mantle to the West of Lake Superior", Bulletin of the Seismological Society of America, 58 #2 (April 1968), 565 - 596.
- Maureau, G. T. "Crustal Structure in Western Canada", M.Sc. Thesis, University of Alberta, 1964.
- Muirhead, K. J. "Eliminating False Alarms when Detecting Seismic Events Automatically", Nature, 217 (February 1968), 533 - 534.
- Smith, Mark K. "Noise Analysis and Multiple Seismometer Theory", Geophysics, XXI #2 (April 1956), 337 - 360.

Warren, D. H., J. H. Healy, J. C. Hoffman, Reinis Kempe,
Srinivasreddy Rauula, and D. J. Stuart. "Technical
Letter #6: Project Early Rise Traveltimes and
Amplitudes", USGS, Menlo Park, 1967.

APPENDIX.

FORTRAN IV PROGRAM FOR THE TIME AND DISTANCE INTEGRALS

The following Fortran IV program was used to calculate the travel time curve for a given earth model. It integrates from R_1 (which is equivalent to r_1 in this paper) to a calculated r_b using velocity model $v(r,0)$, and then has the option of resetting the velocity structure for the up integral by evaluating the $v(r,\theta)$, where θ is twice θ_{sb} .

Two integral formulae were used; and hence the listing of two down integral and two up integral subroutines. One is the center point integration formula and the other is the thin homogeneous shell. A third up integral subroutine, which simply doubles the value of θ_{sb} and T_{sb} , is also listed. This is valid only when $v = v(r)$ and $r_s = r_b$. The appropriate subroutines must be selected by the user.


```

REAL*4 RDEL(50,20),VDEL(50,20),DELMOD(50),RMAN(81),VMAN(81)
REAL*8 R(101),V(101)
REAL*8 RO(101),VO(101)
REAL*8 RADDEG,RE,R1,R2,P3,VRED,TINC,AI1,AI2,AINC,DAI,AI,DELTA,TIME
REAL*8 DELTAC,DELTAM,DELTAP,EM,EP,SLOPE,P,RAD,DELTAK,DELTAD,TRED
REAL*8 V1,PE2,TEST,DR,RADC,RADT,VELC,VELT,RDV,A,THOLD,VEL,TIMEC
100 FORMAT(5F10.0,3I10)
103 FORMAT('ANGLE OF INCIDENCE = ',F10.5)
1040FORMAT('RADIUS OF THE EARTH = ',F10.3,'KM'/'OSTART INTEGRATION AT'
1,F10.3,'KM, STOP AT',F10.3,'KM. RADIUS OF PENETRATION LIMITED TO',
2F10.3,'KM'/' 1/DR STARTS AT',I4,' STOPS AT',I8,' & ITEST =',I8)
1050 FORMAT('ORAY FLUX ON EACH SIDE OF THE RAY IS ',2(D12.6,
1' = LOG ('',F10.5,'') ''), ' AV FLUX =',F10.5)
106 FORMAT('1')
107 FORMAT('1RAY PATH COORDINATES DELETED')
108 FORMAT(2F10.0,I5,54X,I1)
1100FORMAT('-',20X,'RAY STARTS',F8.2,' DEG ',5X,'RAY ENDS',F8.2,
1' DEG ',5X,'INTERVAL NO',I5)
J$=50
I$=20
K$=81
L$=101
RADDEG=3.1415926536D0/180.0D0

C
C DATA CARD 1 F10.0 NRAY
C NRAY IS THE NUMBER OF RAYS PASSED PER SHELL FOR TRAVEL TIME CURVE
C NRAY = 1 IF UNSPECIFIED (BLANK FIELD)
C
READ(5,100)XOUT
NRAY=IFIX(XOUT)
IF(NRAY.LT.2)NRAY=2

C
C DATA CARD 2 F10.0 XOUT
C IF XOUT NOT SPECIFIED, THE RAY PATH CO-ORDINATES ARE DELETED
C IF XOUT NE 0.0 THE RAY PATH CO-ORDINATES ARE CALCULATED
C
READ(5,100)XOUT
IF(IFIX(XOUT).EQ.0)WRITE(6,107)

C
C DATA CARD 3 F10.0 RE
C RE IS THE RADIUS OF THE SPHERE
C RE = 6371.0 (KM) IF UNSPECIFIED
C
READ(5,100)RE
IF(RE.EQ.0.0D0)RE=6371.0D0
2 CONTINUE

C
C DATA CARDS SET 1 TITLE AND DATA OF VELOCITY STRUCTURE
C SEE SUBROUTINE DATA
C
CALL DATA(RDEL,VDEL,DELMOD,J$,I$,RMAN,VMAN,K$,R,V,L$)
1 CONTINUE

C
C DATA CARD SET 1 + 4 5F10.0,3I10 R1,R2,R3,VRED,TINC,IDR1,IDR2,ITEST

```



```

C   R1 IS RADIUS (KM) OF SOURCE
C   RE IS RADIUS (KM) OF SPHERE
C   R1 = RE IF UNSPECIFIED
C   R3 IS RADIUS (KM) OF RECEIVER
C   R3 = RE IF UNSPECIFIED
C   R2 IS MINIMUM RADIUS (KM) RAY MAY PENETRATE
C   VRED IS REDUCTION VELOCITY (KM/SEC) FOR REDUCED TRAVEL TIME
C   VRED = 8.5 KM/SEC IF UNSPECIFIED
C   IDR1 IS IDR AT START OF INTEGRAL
C   WHERE DR = 1/IDR , IS THE INCREMENT IN THE INTEGRAL
C   IDR1 = 2 IF UNSPECIFIED
C   IDR2 IS IDR LIMIT FOR END OF INTEGRAL
C   IDR2 = 128 IF UNSPECIFIED
C   ITEST IS NUMBER OF INCREMENTS TO BOTTOM OF RAY (REND) BEFORE
C   IDR = IDR*2
C   ITEST = 100 IF UNSPECIFIED

```

```

READ(5,100)R1,R2,R3,VRED,TINC,IDR1,IDR2,ITEST

```

```

IF(R1.EQ.0.000)R1=RE

```

```

IF(R3.EQ.0.000)R3=RE

```

```

IF(VRED.EQ.0.000)VRED=8.500

```

```

IF(TINC.EQ.0.000)TINC=0.500

```

```

IF(IDR1.EQ.0)IDR1=2

```

```

IF(IDR2.EQ.0)IDR2=128

```

```

IF(ITEST.EQ.0)ITEST=100

```

```

WRITE(6,104)PE,R1,R3,R2,IDR1,IDR2,ITEST

```

```

3  CONTINUE

```

```

DATA CARD SET 1 + 5 2F10.0,I5,54X,I1  AI1,AI2,NRAYS,ISTOP

```

```

IF (ISTOP = 9 , TERMINATE PROGRAM

```

```

IF (ISTOP = 8 , RE-ENTER PROGRAM AT DATA CARD SET 1 + 4

```

```

IF (ISTOP = 7 , RE-ENTER PROGRAM AT DATA CARD SET 1

```

```

AI1 IS MAXIMUM ANGLE OF INCIDENCE (DEGREES)

```

```

AI2 IS MINIMUM ANGLE OF INCIDENCE (DEGREES)

```

```

IF AI1 IS UNSPECIFIED, AI1 = 89.5, AI2 = 20.0

```

```

NRAYS IS NUMBER OF RAYS PASSED PER SHELL FOR FLUX CALCULATION

```

```

NRAYS = NRAY IF NRAYS.LE.NRAY AND RAY FLUX IS DELETED

```

```

*****RAY FLUX CALCULATED ONLY IF NRAYS.GT.NRAY*****

```

```

READ(5,108)AI1,AI2,NRAYS,ISTOP

```

```

IF(ISTOP.EQ.9)CALL EXIT

```

```

IF(ISTOP.EQ.8)GO TO 1

```

```

IF(ISTOP.EQ.7)GO TO 2

```

```

IF(AI1.GT.90.000)AI1=90.000

```

```

IF(AI1)1010,1010,1011

```

```

1010 CONTINUE

```

```

AI1 = 89.500

```

```

AI2=20.000

```

```

1011 CONTINUE

```

```

AI1=AI1*RADDEG

```

```

AI2=AI2*RADDEG

```

```

IF(NRAYS.LT.NRAY)NRAYS=NRAY

```

```

CALL SET(RDEL,VDEL,J$,I$,RMAN,VMAN,K$,RO,VO,L$,1,IDIMC)

```

```

IDIMOM = IDIMC - 1

```



```

INTR = 1
DO 1000 I = 2, IDIMOM
AI=(R0(I)*V0(I))/(V0(I)*R0(I))
IF(AI.GT.1.000)GO TO 1000
AI=DARSIN(AI)
IF(AI.GT.AI1)GO TO 1000
IF(AI.LT.AI2)AI=AI2
AINC=(AI1-AI)/DFLOAT(NRAYS-1)
DAI=0.1000*RADDEG
IF(AINC.LT.DAI)DAI=AINC
IF(NRAYS.EQ.NRAY)DAI=0.000
INTRVL = I - 1
IF (INTR .NE. INTRVL) GO TO 1001
ANGLE1=AI1/RADDEG
ANGLE2=AI/RADDEG
WRITE(6,110)ANGLE1,ANGLE2,INTRVL
DO 1001 II=1,NRAYS
IA=II-1
AI=AI1-AINC*DFLOAT(IA)
AI=AI/RADDEG
WRITE(6,103)AI
AI=AI1-AINC*DFLOAT(IA)
IF(II.EQ.1)AI=AI-1.0D-8
IF(II.EQ.NRAYS)AI=AI+1.0D-8
IOUT=IFIX(XOUT)
OCALL RAY (RDEL,VDEL,DELMOD,J$,I$,RMAN,VMAN,K$,R,V,L$,AI,R1,R2,R3,
1VRD,TINC,IOUT,IDR1,IDR2,ITEST,RADDEG,DELTA,TIME,RE,P)
DELTAC=DELTA
TIMEC=TIME
IF(DAI.EQ.0.000)GO TO 5
IC=1
OCALL D VEL(R,V,L$,
1R3,V1,IC,IDIM)
C
C
C
V1=ANGLE OF EMERGENCE
V1=DARSIN(P*V1/R3)
DELTAC=DELTA
AI=AI1-AINC*DFLOAT(IA)-DAI
IOUT=0
OCALL RAY (RDEL,VDEL,DELMOD,J$,I$,RMAN,VMAN,K$,R,V,L$,AI,R1,R2,R3,
1VRD,TINC,IOUT,IDR1,IDR2,ITEST,RADDEG,DELTA,TIME,RE,P)
DELTAM=DELTA
IF(II.EQ.1)GO TO 1012
AI=AI1-AINC*DFLOAT(IA)+DAI
OCALL RAY (RDEL,VDEL,DELMOD,J$,I$,RMAN,VMAN,K$,R,V,L$,AI,R1,R2,R3,
1VRD,TINC,IOUT,IDR1,IDR2,ITEST,RADDEG,DELTA,TIME,RE,P)
1012 CONTINUE
DELTAP=DELTA
EP=DABS(DAI*RADDEG)*DSIN(AI1*RADDEG)/DCOS(V1)
EM=EP/(DSIN((DELTAC+DELTAM)/2.000)*DABS(DELTAC-DELTAM))
EP=EP/(DSIN((DELTAC+DELTAP)/2.000)*DABS(DELTAC-DELTAP))
EMLOG=EM
EMLOG=ALOG10(EMLOG)

```



```
EPLOG=EP
EPLOG=ALOG10(EPLOG)
AI=AI1-AINC*DFLOAT(IA)
DIST=DELTAC*RE
TRED=(TIMEC-DELTAC*RE/VRED)
IF(II.EQ.1)EPLOG=EMLOG
IF(II.EQ.NRAYS)EMLOG=EPLOG
FLUX=(EPLOG+EMLOG)/2.0
WRITE(6,105)EP,EPLOG,EM,EMLOG,FLUX
MODEL1=1
5 CONTINUE
1001 CONTINUE
INTR = INTRVL +1
AI1=AI
1000 CONTINUE
GO TO 3
END
```



```

OSUBROUTINE RAY(RDEL,VDEL,DELMOD,J$,I$,RMAN,VMAN,K$,R,V,L$,
1AI,R1,R2,R3,VRED,TINC,IOUT,IDR1,IDR2,ITEST,RADDEG,DELTA,TIME,RE,P)

```

```

CALCULATES TIME, DISTANCE AND RAY PATH FOR A RAY OF GIVEN ANGLE
OF INCIDENCE

```

```

REAL*4 RDEL(J$,I$),VDEL(J$,I$),DELMOD(J$),RMAN(K$),VMAN(K$)
REAL*8 R(L$),V(L$)
REAL*8 RADDEG,RE,R1,R2,R3,VRED,TINC,AI1,AI2,AINC,DAI,AI,DELTA,TIME
REAL*8 DELTAC,DELTAM,DELTAP,EM,EP,SLOPE,P,RAD,DELTAK,DELTAD,TRED
REAL*8 V1,PE2,TEST,DR,RADC,RADT,VELC,VELT,RDV,A,THOLD,VEL,REND
1000FORMAT('0',5X,'DELTA =',F8.2,'KM  T-DELTA/',F4.2,' = ',F7.2,
1' SEC  RAD BTM =',F7.2,'KM')
1020FORMAT('+',78X,'DELTA =',F8.2,'KM  T-DELTA/',F4.2,' = ',
1F7.2,' SEC')
MODEL=1
OIF(MODEL.NE.MODEL1)CALL SET(RDEL,VDEL,J$,I$,RMAN,VMAN,K$,R,V,L$,
1MODEL,IDIM)
MODEL=1
P=0.000
DELTA=0.000
TIME=0.000
THOLD=0.000
IF(AI.GE.90.000*RADDEG)RETURN
OCALL DOWN I(R,V,L$,
1AI,R1,R2,R3,IDR1,IDR2,ITEST,IDIM,IOUT,DELTA,TIME,RE,P,RAD,THOLD,
2TINC,IDR,IFEFLT,REND)
DELTAK=RE*DELTA
DELTAD=DELTA/RADDEG
TRED=TIME-DELTAK/VRED
WRITE(6,100) DELTAK,VRED,TRED,RAD
DELTAK=DELTAK+DELTAK
IC=1
OCALL D VEL(R,V,L$,
1REND,PE2,IC,IDIM)
IF(IFEFLT.NE.0)PE2=DARSIN(P*PE2/REND)
OCALL MOD(DELMOD,J$,
1DELTAK,MODEL)
OIF(MODEL.NE.MODEL1)CALL SET(RDEL,VDEL,J$,I$,RMAN,VMAN,K$,R,V,L$,
1MODEL,IDIM)
2 CONTINUE
IF(MODEL.EQ.MODEL1)GO TO 5
IC=1
OCALL D VEL(R,V,L$,
1REND,V1,IC,IDIM)
IF(IFEFLT.EQ.0)P=REND/V1
IF(IFEFLT.NE.0)P=(REND/V1)*DSIN(PE2)
5 CONTINUE
IDR=1
DO 3 I=1,IDR2
IDR=IDR*2
IF(IDR.GE.IDR2)GO TO 4
3 CONTINUE
4 CONTINUE

```



```
1 CONTINUE
  OCALL UP I(R,V,L$,
  1AI,R1,R2,R3,IDR1,IDR2,ITEST,IDIM,IOUT,DELTA,TIME,RE,P,RAD,THOLD,
  2TINC,IDR,IREFLT,REND)
  IDR=IDR1
  RAD=R1
  DELTAK=RE*DELTA
  DELTAD=DELTA/RADDEG
  TRED=TIME-DELTAK/VRED
  WRITE(6,102) DELTAK,VRED,TRED
  RETURN
END
```



```

OSUBROUTINE DOWN I(R,V,L$,
1AI,R1,R2,R3,IDR1,IDR2,ITEST,IDIM,IOUT,DELTA,TIME,RE,P,RAD,THOLD,
2TINC,IDR,IREFLT,REND)

```

```

    INTEGRATES FROM R1 TO REND (RAY BOTTOM)
    USING CENTER POINT INTEGRATION FORMULA

```

```

    REAL*8 R(L$),V(L$)
    REAL*8 RADDEG,RE,R1,R2,R3,VRED,TINC,AI1,AI2,AINC,DAI,AI,DELTA,TIME
    REAL*8 DELTAC,DELTAM,DELTAP,EM,EP,SLOPE,P,RAD,DELTAK,DELTAD,TRED
    REAL*8 V1,PE2,TEST,DR,RADC,RADT,VELC,VELT,RDV,A,THOLD,VEL,REND
100 FORMAT(1X,5(7X,'X',7X,'Z',7X,'T'))
101 FORMAT(8(1X,D14.8))
    IC=1
    ID=0
    IF(P1.EQ.0.000)P1=R(1)
    OCALL D VEL(R,V,L$,
1R1,V1,IC,IDIM)
    IF(P.EQ.0.000)P=(R1/V1)*DSIN(AI)
    PE2=P*P
    CALL BOTTOM(R,V,IDIM,P,AI,REND,IREFLT)
    RAD=R1
    IT=IC
    TEST=DFLOAT(ITEST)
    IDR=IDR1
    DR=1/DFLOAT(IDR)
    IF(IOUT.EQ.1)WRITE(6,100)
4 CONTINUE
    RADC=RAD-DR/2.000
    RADT=RAD-DR*TEST
    OCALL D VEL(R,V,L$,
1RADC,VELC,IC,IDIM)
    OCALL D VEL(R,V,L$,
1RADT,VELT,IT,IDIM)
    IF(RADT/VELT.LE.P)GO TO 1
    IF(RADT/VELC.LE.P)GO TO 2
    IF(RAD-DR.LT.R2)GO TO 3
    RDV=RADC/VELC
    A=RDV*RDV-PE2
    A=DR/DSQRT(RDV*RDV-PE2)
    DELTA=DELTA+P*A/RADC
    TIME=TIME+RDV*A/VELC
    RAD=RAD-DR
    IF(IOUT.EQ.1)CALL OUT(DELTA,TIME,RE,TINC,THOLD,RAD,ID,0)
    GO TO 4
1 CONTINUE
2 CONTINUE
    IT=1
    IDR=IDR*2
    DR=1/DFLOAT(IDR)
    IF(TEST.EQ.1.000)GO TO 5
    IF(IDR.GE.IDR2)TEST=1.000
    GO TO 4
5 CONTINUE

```



```

      IF(IOUT.EQ.1)CALL OUT(DELTA,TIME,RE,TINC,THOLD,RAD,ID,1)
      RETURN
3  CONTINUE

      MODIFY LAST STEP IN INTEGRATION TO THIN HOMOGENEOUS SHELL FORMULA
      USE THIS FORMULA ONLY IF IREFLT =0
      OTHERWISE RETAIN PRESENT FORM

      DR=RAD-R2
      RADC=RAD-DR/2.000
      0CALL DVEL(R,V,L$,
      1RADC,VELC,IC,IDIM)
      RDV=RADC/VELC
      IF(RDV*RDV-PE2.LE.0.000)GO TO 6
      A=DR/DSQRT(RDV*RDV-PE2)
      DELTA=DELTA+P*A/RACC
      TIME=TIME+RDV*A/VELC
      RAD=RAD-DR
6  CONTINUE
      IF(IOUT.EQ.1)CALL OUT(DELTA,TIME,RE,TINC,THOLD,RAD,ID,1)
      RETURN
      END

```



```

OSUBROUTINE UP I(R,V,L$,
1AI,R1,R2,R3,IDR1,IDR2,ITEST,IDIM,IOUT,DELTA,TIME,RE,P,RAD,THOLD,
2TINC,IDR,IREFLT,REND)

```

```

C
C   INTEGRATES FROM REND (RAY BOTTOM) TO R3
C   USING CENTER POINT INTEGRATION FORMULA
C

```

```

REAL*8 R(L$),V(L$)
REAL*8 RADDEG,RE,R1,R2,R3,VRED,TINC,AI1,AI2,AINC,DAI,AI,DELTA,TIME
REAL*8 DELTAC,DELTAM,DELTAP,EM,EP,SLOPE,P,RAD,DELTAK,DELTAD,TRED
REAL*8 V1,PE2,TEST,DR,RADC,RADT,VELC,VELT,RDV,A,THOLD,VEL,REND
100 FORMAT(1X,5(7X,'X',7X,'Z',7X,'T'))
101 FORMAT(8(1X,D14.8))

```

```

IC=1
ID=0
OCALL U VEL(R,V,L$,
1RAD,VEL,IC,IDIM)
IF(P.EQ.0.000)P=(RAD/VEL)*DSIN(AI)
PE2=P*P
IF(R3.EQ.0.000)R3=R(1)
IT=1
TEST=DFLOAT(ITEST)
DR=1/DFLOAT(IDR)
IF(IOUT.EQ.1)WRITE(6,100)

```

```

C
C   MODIFY FIRST STEP IN INTEGRATION TO THIN HOMOGENEOUS SHELL FORMULA
C   USE THIS FORMULA ONLY IF IREFLT =0
C   OTHERWISE RETAIN PRESENT FORM
C

```

```

4 CONTINUE
RADC=RAD+DR/2.000
RADT=RAD-DR*TEST
OCALL U VEL(R,V,L$,
1RADC,VELC,IC,IDIM)
OCALL U VEL(R,V,L$,
1RADT,VELT,IT,IDIM)
IF(RADT/VELT.GT.P)GO TO 1
IF(RADT/VELC.GT.P)GO TO 2
IF(RAD+DR.GE.R3)GO TO 3
RDV=RADC/VELC
A=RDV*RDV-PE2
A=DR/DSQRT(RDV*RDV-PE2)
DELTA=DELTA+P*A/RADC
TIME=TIME+RDV*A/VELC
RAD=RAD+DR
IF(IOUT.EQ.1)CALL OUT(DELTA,TIME,RE,TINC,THOLD,RAD,ID,0)
GO TO 4
1 CONTINUE
2 CONTINUE
IDR=IDR/2
DR=1/DFLOAT(IDR)
IT=1
IF(IDR.GT.IDR1)GO TO 4
DR=1/DFLOAT(IDR1)

```



```
TEST=RAD/DR
GO TO 4
3 CONTINUE
DR=P3-RAD
RADC=RAD+DR/2.000
0CALL UVEL(R,V,L$,
1RADC,VELC,IC,IDIM)
RDV=RADC/VELC
IF(RDV*RDV-PE2.LE.0.000)GO TO 5
A=DR/DSQRT(RDV*RDV-PE2)
DELTA=DELTA+P*A/RADC
TIME=TIME+RDV*A/VELC
RAD=RAD+DR
5 CONTINUE
IF(IOUT.EQ.1)CALL OUT(DELTA,TIME,RE,TINC,THOLD,RAD,ID,1)
RETURN
END
```



```

SUBROUTINE DOWN I(R,V,L$,
1AI,R1,R2,R3,IDR1,IDR2,ITEST,IDIM,IOUT,DELTA,TIME,RE,P,RAD,THOLD,
2TINC,IDR,IREFLT,REND)

```

```

INTEGRATES FROM R1 TO REND (RAY BOTTOM)
USING THIN HOMOGENEOUS SHELL FORMULA

```

```

REAL*8 R(L$),V(L$)
REAL*8 V1,PE2,TEST,DR,RADC,RADT,VELC,VELT,RDV,A,THOLD,VEL
REAL*8 DELTAC,DELTAM,DELTAP,EM,EP,SLOPF,P,RAD,DELTAK,DELTAD,TRFD
REAL*8 RADDEG,RE,R1,R2,R3,VRED,TINC,AI1,AI2,AINC,DAI,AI,DELTA,TIME
REAL*8 RHOLD,PEND,DRD2,RADMDR,RADPDR,PVC,PVCE2
IC = 1
ID = 0
IDR2D2=IDR2/2
DELTA = 0.000
TIME = 0.000
IF(R1 .LE. 0.000) R1 = R(1)
RHOLD =R1
CALL D VEL (R,V,L$,R1,V1,IC,IDIM)
IF ( P .EQ. 0.000) P = R1*DSIN(AI)/V1
PE2 = P*P
CALL BOTTOM (R,V,ICIM,P,AI,REND,IREFLT)
TEST = DFLOAT(ITEST)
IF(IREFLT .EQ. 1) TEST = 0.000
RAD = R1
IDR = IDR1
3 CONTINUE
DR = 1.000/DFLOAT(IDR)
DRD2 = DR/2.000
I = 0
1 CONTINUE
I = I + 1
RADC = RAD -DRD2
RADMDR =RHOLD - FLCAT(I)*DR
IF(RADMDR -TEST*DR .LE. REND) GO TO 4
CALL D VEL (R,V,L$,RADC,VELC,IC,IDIM)
PVC = P * VELC
PVCE2 = PVC * PVC
DELTA = DELTA+DARCOS(PVC/RAD)-DARCOS(PVC/RADMDR)
TIME = TIME+(DSQRT(RAD*RAD-PVCE2)-DSQRT(RADMDR*RADMDR-PVCE2))/VELC
RAD = RADMDR
GO TO 1
4 CONTINUE
IF (IREFLT .EQ. 1) GO TO 2
RHOLD = RAD
I = 0
IDR = IDR*2
IF(IDR .LE. IDR2D2)TEST=0.000
IF (IDR .LE. IDR2) GO TO 3
2 CONTINUE
DR =(RAD -PEND)/2.000
DRD2=DR /2.000
RADC = RAD - DRD2

```



```
CALL D VEL (R,V,L$,RADC,VFLC,IC,IDIM)
PVC = P* VELC
PVCE2=PVC * PVC
DELTA=DELTA+DARCOS(PVC/RAD)
TIME=TIME+(DSQRT(RAD*RAD-PVCE2))/VELC
IF(IREFLT.EQ.0)GO TO 5
DELTA=DELTA-DARCOS(PVC/REND)
TIME=TIME-DSQRT(REND*REND-PVCE2)/VELC
5 CONTINUE
RAD = REND
RETURN
END
```



```

SUBROUTINE UP (R,V,L$,
1AI,P1,R2,R3,IDR1,IDR2,ITEST,IDIM,IOUT,DELTA,TIME,RE,P,RAD,THOLD,
2TINC,IDR,IREFLT,REND)

```

```

INTEGRATES FROM REND (RAY BOTTOM) TO R3
USING THIN HOMOGENEOUS SHELL FORMULA

```

```

REAL*8 R(L$),V(L$)
REAL*8 RADDEG,RE,P1,R2,R3,VRED,TINC,AI1,AI2,AINC,DAI,AI,DELTA,TIME
REAL*8 DELTAC,DELTAM,DELTAP,EM,FP,SLOPE,P,RAD,DELTAK,DELTAD,TRED
REAL*8 V1,PE2,TEST,DR,RADC,RADT,VELC,VELT,RDV,A,THOLD,VEL
REAL*8 RHOLD,REND,DRD2,RADMDR,RADPDR,PVC,PVCE2
TEST = DFLOAT(ITEST)
IC = 1
ID = 0
IDR=IDR2
DR=1.000/DFLOAT(IDR)
DRD2=DR/2.000
RADC=RAD+DRD2
CALL U VEL (R,V,L$,RADC,VELC,IC,IDIM)
IF(PVC/RAD.LT.1.000)GO TO 5
RADPDR=RAD+DR
PVC=P*VELC
PVCE2=PVC*PVC
DELTA=DELTA+DARCOS(PVC/RADPDR)
TIME=TIME+(DSQRT(RADPDR*RADPDR-PVCE2))/VELC
RAD=RADPDR
5 CONTINUE
CALL U VEL(R,V,L$,RAD,VEL,IC,IDIM)
IF(P.NE.0.000)GO TO 4
P=RAD*DSIN(AI)/VEL
IREFLT=2
4 CONTINUE
IF(IREFLT.EQ.0)P=RAD/VEL
IF(RAD/VEL.LT.P)P=RAD/VEL
PE2 = P*P
IF (R3 .LE. 0.000) R3 = R(1)
I = 0
3 CONTINUE
RHOLD = RAD
DR = 1.000/DFLOAT(IDR)
DRD2 = DR/2.000
2 CONTINUE
RADC = RAD + DRD2
I = I + 1
RADPDR = RHOLD + FLOAT(I)*DR
IF (RADPDR .GE. R3) GO TO 1
CALL U VEL(R,V,L$,RADC,VELC,IC,IDIM)
PVC = P*VELC
PVCE2 = PVC * PVC
DELTA =DELTA+DARCOS(PVC/RADPDR)-DARCOS(PVC/RAD)
TIME=TIME+(DSQRT(RADPDR*RADPDR-PVCE2)-DSQRT(RAD*RAD-PVCE2))/VELC
RAD = RADPDR
IF (RAD -TEST*DR .GT. REND) GO TO 2

```



```
IDR = IDR/2
I = 0
IF(IDR .GT. IDR1) GO TO 3
IDR = IDR1
DR = 1.000/DFLOAT(IDR)
TEST = RAD/DR
GO TO 3
1 CONTINUE
IDR = IDR1
DR = R3 - RAD
DRD2 = DR/2.000
RADC = (R3+RAD)/2.000
CALL U VEL (R,V,L$,RADC,VELC,IC,IDIM)
PVC = P* VELC
PVCE2 = PVC*PVC
DELTA = DELTA+(DARCOS(PVC/R3)-DARCOS(PVC/RAD))
TIME = TIME+(DSQRT(R3*R3-PVCE2)-DSQRT(RAD*RAD-PVCE2))
RAD = R3
IDR = IDR1
RETURN
END
```



```

OSUBROUTINE UP I(R,V,L$,
1AI,R1,R2,R3,IDR1,IDR2,ITEST,IDIM,IDUT,DELTA,TIME,RE,P,RAD,THOLD,
2TINC,IDR,IREFLT,REND)

```

```

C      INTEGRATES FROM REND (RAY BOTTOM) TO R3

```

```

C      ****ASSUMING      R3 = R1

```

```

C      ****ASSUMING      SAME VELOCITY STRUCTURE AS USED IN DOWN I

```

```

C      *****NOTE***** THIS ROUTINE DOES NOT CALCULATE RAY PATH ***

```

```

C      REAL*8 R(L$),V(L$)

```

```

C      REAL*8 RADDEG,RE,R1,R2,R3,VRED,TINC,AI1,AI2,AINC,DAI,AI,DELTA,TIME

```

```

C      REAL*8 DELTAC,DELTAM,DELTAP,EM,EP,SLOPE,P,RAD,DELTAK,DELTAD,TRED

```

```

C      REAL*8 V1,PE2,TEST,DR,RADC,RACT,VELC,VELT,RDV,A,THOLD,VEL,REND

```

```

100  FORMAT(1X,5(7X,'X',7X,'Z',7X,'T'))

```

```

101  FORMAT(8(1X,D14.8))

```

```

C      DELTA=DELTA+DELTA

```

```

C      TIME=TIME+TIME

```

```

C      RAD=R1

```

```

C      IDR=IDR1

```

```

C      RETURN

```

```

C      END

```



```

OSUBROUTINE D VEL(R,V,L$,
1RAD,VEL,IC,IDIM)

```

```

C
C   CALCULATES VELOCITY AT A GIVEN RADIUS FOR DECREASING R
C   USING LINEAR INTERPOLATION FORMULA BETWEEN V(I), V(I+1)
C   WHERE      R(I).GT.R.GE.R(I+1)
C

```

```

REAL*8 R(L$),V(L$)
REAL*8 RADDEG,RE,R1,R2,R3,VRED,TINC,AI1,AI2,AINC,DAI,AI,DELTA,TIME
REAL*8 DELTAC,DELTAM,DELTAP,EM,EP,SLOPE,P,RAD,DELTAK,DELTAD,TRED
REAL*8 V1,PE2,TEST,DR,RADC,RADT,VELC,VELT,RDV,A,THOLD,VFL
IF(RAD.GE.R(1))GO TO 1
ISTART=IC
IDIM1=IDIM-1
DO 2 I=ISTART,IDIM1
IC=I
IP1=I+1
IF(RAD.GE.R(IP1))GO TO 3
2 CONTINUE
3 CONTINUE
VEL=((V(IP1)-V(I))*RAD+V(I)*R(IP1)-V(IP1)*R(I))/(R(IP1)-R(I))
RETURN
1 CONTINUE
VEL=V(1)
IC=1
RETURN
END

```



```

OSUBROUTINE U VEL(R,V,L$,
1RAD,VEL,IC,IDIM)

```

```

C
C   CALCULATES VELOCITY AT A GIVEN RADIUS FOR INCREASING R
C   USING LINEAR INTERPOLATION FORMULA BETWEEN V(I), V(I+1)
C   WHERE      R(I).GT.R.GE.R(I+1)
C

```

```

REAL*8 R(L$),V(L$)
REAL*8 RADDEG,RE,R1,R2,R3,VRED,TINC,AI1,AI2,AINC,DAI,AI,DELTA,TIME
REAL*8 DELTAC,DELTAM,DELTAP,EM,EP,SLOPE,P,RAD,DELTAK,DELTAD,TRED
REAL*8 V1,PE2,TEST,DR,RADC,RADT,VELC,VELT,RDV,A,THOLD,VEL
ISTART=IC
DO 1 I=ISTART,IDIM
  J=IDIM-I+1
  IC=I
  IF(RAD.LT.R(J))GO TO 2
1 CONTINUE
2 CONTINUE
  IF(RAD.GT.R(1))GO TO 3
  I=J
  IP1=J+1
  VEL=((V(IP1)-V(I))*RAD+V(I)*R(IP1)-V(IP1)*R(I))/(R(IP1)-R(I))
  RETURN
3 CONTINUE
  VEL=V(1)
  RETURN
END

```



```
OSUBROUTINE SET(RDEL,VDEL,J$,I$,RMAN,VMAN,K$,R,V,L$,
1MODEL,IDIM)
```

```
SETS R,V TO RDEL,VDEL,RMAN,VMAN ASSUMING NUMBER 'MODEL'
```

```
REAL*8 R(L$),V(L$)
```

```
REAL*4 RDEL(J$,I$),VDEL(J$,I$),RMAN(K$),VMAN(K$)
```

```
REAL*8 RADDEG,RF,R1,R2,R3,VRED,TINC,AI1,AI2,AINC,DAI,AI,DELTA,TIME
```

```
REAL*8 DELTAC,DELTAM,DELTAP,EM,EP,SLOPE,P,RAD,DELTAK,DELTAD,TRED
```

```
REAL*8 V1,PE2,TEST,DR,RADC,RADT,VELC,VELT,RDV,A,THOLD,VEL
```

```
DO 1 I=1,I$
```

```
IF(RDEL(MODEL,I).LE.0.0)GO TO 2
```

```
II=I
```

```
R(II)=DFLOAT(IFIX((RDEL(MODEL,II)*1.0E2)+0.5))/1.0D2
```

```
V(II)=DFLOAT(IFIX((VDEL(MODEL,II)*1.0E4)+0.5))/1.0D4
```

```
1 CONTINUE
```

```
2 CONTINUE
```

```
II=II+1
```

```
L$M1=L$-1
```

```
DO 3 I=II,L$M1
```

```
J=I-II+1
```

```
IF(RMAN(J).LE.0.0)GO TO 4
```

```
IDIM=I
```

```
R(I)=DFLOAT(IFIX((RMAN(J)*1.0E2)+0.5))/1.0D2
```

```
V(I)=DFLOAT(IFIX((VMAN(J)*1.0E4)+0.5))/1.0D4
```

```
3 CONTINUE
```

```
4 CONTINUE
```

```
IDIM=IDIM+1
```

```
R(IDIM)=0.0D0
```

```
V(IDIM)=V(IDIM-1)
```

```
100 FORMAT(1X,10F13.5)
```

```
RETURN
```

```
END
```



```

OSUBROUTINE MOD(DELMOD,J$,
1DELTAK,MODEL)

```

```

C
C   CALCULATES MODEL NUMBER (MODEL) FOR A GIVEN RANGE FROM SOURCE
C

```

```

REAL*8 RADDEG,RE,R1,R2,R3,VRED,TINC,AI1,AI2,AINC,DAI,AI,DELTA,TIME

```

```

REAL*8 DELTAC,DELTAM,DELTAP,EM,EP,SLOPE,P,RAD,DELTAK,DELTAD,TPED

```

```

REAL*8 V1,PE2,TFST,DR,RADC,RADT,VELC,VELT,RDV,A,THOLD,VEL

```

```

REAL*4 DELMOD(J$)

```

```

DO 1 I=1,J$

```

```

MODEL=I

```

```

IF(DELTAK.LE.DELMOD(I))RETURN

```

```

1 CONTINUE

```

```

RETURN

```

```

END

```



```
SUBROUTINE OUT(DELTA,TIME,RE,TINC,THOLD,RAD,ID,IDUMP)
```

```
  OUTPUTS RAY PATH CO-ORDINATES X,Z,T
```

```
  MODIFY FOR CALCOMP PLOT OUTPUT
```

```
  REAL*4 X(5),Z(5),T(5)
```

```
  REAL*8 RADDEG,RE,R1,R2,R3,VRED,TINC,AI1,AI2,AINC,DAI,AI,DELTA,TIME
```

```
  REAL*8 DELTAC,DELTAM,DELTAP,EM,EP,SLOPE,P,RAD,DELTAK,DELTAD,TRED
```

```
  REAL*8 V1,PE2,TEST,DR,PADC,RACT,VELC,VELT,RDV,A,THOLD,VEL
```

```
100 FORMAT(1X,5(2F8.1,F8.2))
```

```
  IF(IDUMP.EQ.1)GO TO 1
```

```
  IF(TIME-THOLD.LT.TINC)RETURN
```

```
  ID=ID+1
```

```
  X(ID)=RAD*DSIN(DELTA)
```

```
  Z(ID)=RE-RAD*DCOS(DELTA)
```

```
  T(ID)=TIME
```

```
  THOLD=THOLD+TINC
```

```
  IF(ID.LT.5)RETURN
```

```
  WRITE(6,100)((X(K),Z(K),T(K)),K=1,ID)
```

```
  ID=0
```

```
  RETURN
```

```
1 CONTINUE
```

```
  ID=ID+1
```

```
  X(ID)=RAD*DSIN(DELTA)
```

```
  Z(ID)=RE-RAD*DCOS(DELTA)
```

```
  T(ID)=TIME
```

```
  WRITE(6,100)((X(K),Z(K),T(K)),K=1,ID)
```

```
  ID=0
```

```
  RETURN
```

```
END
```



```
SUBROUTINE DATA(RDEL,VDEL,DELMOD,J$,I$,RMAN,VMAN,K$,R,V,L$)
```

```
READS VELOCITY STRUCTURE DATA CARDS SET 1
```

```
REAL*8 R(L$),V(L$)
```

```
REAL*4 RDEL(J$,I$),VDEL(J$,I$),DELMOD(J$),RMAN(K$),VMAN(K$)
```

```
REAL*8 RADDEG,RE,R1,R2,R3,VRED,TINC,AI1,AI2,AINC,DAI,AI,DELTA,TIME
```

```
REAL*8 DELTAC,DELTAM,DELTAP,EM,EP,SLOPE,P,RAD,DELTAK,DELTAD,TRED
```

```
REAL*8 V1,PE2,TEST,DR,RADC,RADT,VELC,VELT,RDV,A,THOLD,VEL
```

```
1000FORMAT('1RAY PATHS & TRAVEL TIME CURVE FOR A SPHERICALLY SYMMETRIC  
1 EARTH')
```

```
1010FORMAT(1X,'
```

```
1',I1)
```

```
102 FORMAT(8F10.0)
```

```
103 FORMAT('0',5(6X,'RADIUS',4X,'VELOCITY'))
```

```
104 FORMAT(1X,10F12.5)
```

```
105 FORMAT(' MODEL',I4,' USED FOR DELTA LESS THAN',F10.1,'KM')
```

```
106 FORMAT(' MODEL',I4,' USED FOR DELTA LESS THAN',F14.8,'KM')
```

```
107 FORMAT('1MODEL',I5)
```

```
WRITE(6,100)
```

```
DO 1 J=1,50
```

```
DATA CARDS SET 1.1 TERMINATED WITH 9 IN COLUMN 80  
THESE CARDS CONTAIN THE TITLE TO THE CRUSTAL VELOCITY STRUCTURE  
EACH CARD IS REPRODUCED IN THE OUTPUT
```

```
2 CONTINUE
```

```
READ(5,101)ISTOP
```

```
WRITE(6,101)
```

```
IF(ISTOP.NE.9)GO TO 2
```

```
DATA CARDS SET 1.2(1 CARD) F10.0 DELMOD(J) J=1 INITIALLY  
AZIMUTH RANGE (KM) OF MODEL J LIES BETWEEN DELMOD(J-1),DELMOD(J)
```

```
READ(5,102)DELMOD(J)
```

```
WRITE(6,105)J,DELMOD(J)
```

```
DO 3 I=1,20,4
```

```
N=I+3
```

```
DATA CARDS SET 1.3 8F10.0 RDEL,VDEL OF MODEL J  
TERMINATED BY READING 5 CARDS OR LAST RDEL OF CARD LE.0.0  
IF RMAN (LAST OF CARD) IS LT 0.0 GO ON TO DATA CARDS SET 1.4  
IF PDEL (LAST OF CARD) IS 0.0,READ NEXT DELMOD AND RMAN,VMAN  
BY READING NEXT SET OF DATA CARDS SET 1.1, 1.2, AND 1.3  
THIS CAN BE DONE FOR 50 MODELS AT MOST
```

```
READ(5,102)((RDEL(J,K),VDEL(J,K)),K=1,N)
```

```
IF(RDEL(J,N).LE.0.0)GO TO 4
```

```
3 CONTINUE
```

```
4 CONTINUE
```

```
WRITE(6,103)
```

```
WRITE(6,104)((RDEL(J,K),VDEL(J,K)),K=1,N)
```

```
NMODEL=J
```

```
IF(RDEL(J,N).LT.0.0)GO TO 5
```



```

1 CONTINUE
5 CONTINUE
  DELMOD(NMODEL)=1.0E70
  WRITE(6,106)NMODEL,DELMOD(NMODEL)

C
C DATA CARDS SET 1.4 TERMINATED WITH 9 IN COLUMN 80
C TITLE OF MANTLE VELOCITY STRUCTURE
C

6 CONTINUE
  READ(5,101)ISTOP
  WRITE(6,101)
  IF(ISTOP.NE.9)GO TO 6
  DO 7 I=1,80,4
    N=I+3

C
C DATA CARDS SET 1.5 8F10.0 RMAN,VMAN
C TERMINATED BY READING 10 CARDS OR LAST RMAN OF A CARD LE 0.0
C

  READ(5,102)((RMAN(K),VMAN(K)),K=I,N)
  IF(RMAN(N).LE.0.0)GO TO 8
7 CONTINUE
8 CONTINUE
  N=N-4
  DO 9 I=1,4
    IN=I+N
    IF(RMAN(I).LE.0.0)GO TO 10
9 CONTINUE
10 CONTINUE
  RMAN(IN)=0.0
  IF(VMAN(IN).LE.0.0)VMAN(IN)=VMAN(IN-1)
  WRITE(6,103)
  WRITE(6,104)((RMAN(K),VMAN(K)),K=1,IN)
  DO 11 I=1,NMODEL
    CALL SET(RDEL,VDEL,J$,I$,RMAN,VMAN,K$,R,V,L$,
11, IDIM)
    WRITE(6,107)I
    WRITE(6,103)
    WRITE(6,104)((R(K),V(K)),K=1,IDIM)
11 CONTINUE
  RETURN
  END

```


SUBROUTINE BOTTOM(R,V,IDIM,P,AI,REND,IREFLT)

CALCULATES THE MINIMUM RADIUS (REND) OF A GIVEN RAY

IREFLT = 0 IN CASE OF REFRACTED RAY
IREFLT = 1 IN CASE OF REFLECTED RAY

```

REAL*8 R(IDIM), V(IDIM)
REAL *8 P, AI, REND, A, B, C
IF (P) 3, 2, 3
2 CONTINUE
P= (R(1)*DSIN(AI))/V(1)
3 CONTINUE
IREFLT = 0
IDIMM1 = IDIM - 1
DO 1 I = 1, IDIMM1
IP1 = I + 1
IF(R(IP1) .EQ. R(I)) GO TO 1
B = R(IP1) - R(I)
A = (V(IP1) - V(I))/B
B = (R(IP1) * V(I) - R(I)*V(IP1))/B
REND = (B*P)/(1.000-(A*P))
IF (REND .GE. R(IP1)) GO TO 5
1 CONTINUE
5 CONTINUE
IF (REND .LT. R(I)) GO TO 6
IREFLT = 1
REND = R(I)
6 CONTINUE
RETURN
END

```


B29921